Feedback between stochastic gene networks and population dynamics enables cellular decision making

Paul Piho and Philipp Thomas*
Department of Mathematics, Imperial College London, UK

Phenotypic selection is the process where genetically identical cells are subject to different reproductive abilities due to cellular noise. Such noise arises from fluctuations in the rates by which proteins are synthesised inside living cells and is hypothesised to play a crucial role in how cells make decisions and respond to stress or drugs. Nevertheless, the state-of-the-art modelling tools for quantifying cellular noise, such as the Gillespie algorithm and the chemical master equation, simply ignore selection. Here, we propose a general stochastic agent-based model for growing populations where the feedback of gene expression dynamics and cell cycle progression directly contribute to cell division dynamics. We devise a finite state projection method as a quantitative analysis tool and inference method for single-cell data obtained from mother machines and lineage trees. We use the theory to quantify selection in multi-stable gene expression networks and elucidate that the interplay between gene expression and phenotypic selection enables robust decision-making essential for developmental lineage decisions. Using live-cell data, we demonstrate that combining theory and inference provides quantitative insights into bet-hedging-like response to DNA damage, and adaption during antibiotic tolerance in *Escherichia coli*.

INTRODUCTION

Cells make decisions in response to changes in gene expression, which is surprisingly noisy even among genetically identical cells facing the same environmental conditions [1–3]. Such cellular noise arises from randomness in the biochemical reactions synthesizing proteins. Since these proteins are involved in gene regulatory networks, stochasticity in expression levels can impact cellular functions, cell proliferation, and survival. The interactions between gene networks and population dynamics give rise to phenotypic selection even in clonal populations [3–5]. Phenotypic selection can have functional consequences in development [6, 7], how cells respond to stress [8–10], and drug resistance [11–13]. Understanding these consequences is important to enhance the function of synthetic circuits inside cells [14–16].

The Gillespie algorithm is widely used to simulate stochastic gene expression [1]. The method exactly simulates reaction dynamics at cellular scales, but it implicitly assumes that cells are static and gene expression occurs isolated from dynamic cellular context. Recent studies challenged this static view of cells by examining the effect cell division has on gene expression through mechanisms of partitioning of molecules [17–19]. Some studies showed that when cells compete for growth, the distribution across growing populations differs from isolated lineages as observed in the mother machine [20–22]. An outstanding issue is to quantify how gene expression affects cell division.

It is becoming increasingly clear that gene expression noise contributes to cell-to-cell variation in cellular timings [23–25]. A range of studies have focussed on modelling interdivision time through the expression of a division protein hitting a set target level from a fixed basal level [26–30]. The model recovers correlations in interdivision time and cell size compatible with the adder division rule in bacteria. However, a single division protein consistent with time-lapse observations cannot always be identified, and several cues may contribute to phenotypic selection when cells respond to stress or drugs.

More generally, the coupling of gene expression and cell division involves feedback, where gene expression affects cell division frequency, which modulates expression levels. For example, competition between cells decreases the interdivision time and in turn increases the frequency with which molecules are partitioned at cell division [22]. On the other hand, expression levels of fitness-inducing genes are elevated when they are under selection [31, 32]. Selection due to differences in division rate is thus distinguished from natural selection arising from a competitive advantage of fast-growing subpopulations.

Natural selection can, in principle, be probed through switching off competition. This can be achieved, for example, by culturing cells in a mother machine [33]. Yet differences in division rates are expected to impact expression levels even in isolated cells and can also be engineered artificially [14]. A quantitative theory of the interactions between gene networks and population dynamics is still missing, and it thus remains elusive how to distinguish natural selection from selection on division rate.

We propose a stochastic framework to model cells as agents that divide in response to intracellular stochastic reaction networks. The model allows us to probe how gene expression contributes to cell proliferation and natural selection and how these effects shape gene expression. Specifically, we show that the division distributions in growing cell populations differ from the first-passage distributions of conventional stochastic reaction networks due to the consequences of division rate, natural selection, and cell history. We provide accurate but tractable

* Correspondence to: p.thomas@imperial.ac.uk

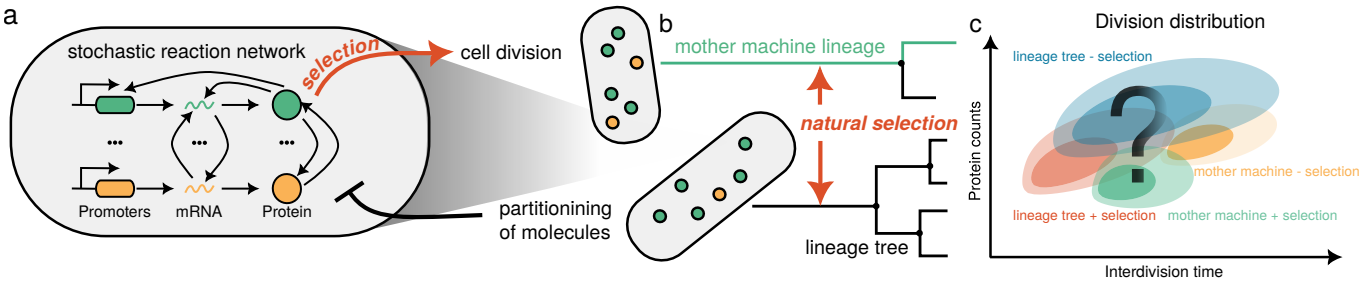

FIG. 1. **Quantifying interactions between gene networks and population dynamics with agent-based modelling of clonal populations (a)** Cartoon of the agent-based model combining intracellular reaction network coupled to cell division. Intracellular reactions affect cell division rate (red arrow) while partitioning of molecules dilutes cellular expression levels (black repressive arrow). **(b)** Lineage statistics of agent-based models measure distributions across lineage tree resulting from competition of cells through natural selection. A mother machine lineage (green line of descendant) follows a single cell in the lineage tree starting from an ancestral and following each daughter cell with equal probability. Mother machine sampling avoids natural selection, i.e., competition of cells for growth (red arrow). **(c)** Illustration of division distributions for a cell to divide at a given age and protein count for a lineage tree of cells including division-rate selection and natural selection (red), a lineage tree without division-rate selection (blue), and the corresponding mother machine lineages (green and yellow).

approximations that provide insights into wide ranges of parameter space and allow us to quantify selection effects from time-lapse observation data.

RESULTS

A. Analytical framework for stochastic agent-based modelling of selection in gene networks

We developed a stochastic agent-based formulation of a growing clonal cell population that couples the internal stochastic gene regulatory dynamics and the population dynamics modelling cell division. In the model, each cell is represented by an agent (Figure 1a) that contains a gene regulatory network composed of biochemical species $X_1, \cdots, X_{N_s}$ that react through R intracellular reactions. Consequently, the state of each cell is given by its age τ and the molecular content $\boldsymbol{x}$ and cells divide at a $\boldsymbol{x}$-dependent rate $\gamma(\boldsymbol{x}, \tau)$. Such agent-based models of cell populations can be exactly simulated by the extended First Division algorithm (Methods F).

Agent-based stochastic simulations are time- and resource-consuming especially in the context of parameter inference when large numbers of parametrisation need to be checked. We can make analytical progress by considering the long-term behaviour of the mean number of cells $n(\boldsymbol{x}, \tau, t)$ with molecule counts $\boldsymbol{x}$ and age τ that grows exponentially with time t (SI Section S1). Normalising this quantity leads to a stable snapshot distribution $\Pi(\boldsymbol{x}, \tau) = \Pi(\boldsymbol{x}|\tau)\Pi(\tau)$, where $\Pi(\boldsymbol{x}|\tau)$ is the (conditional) snapshot distribution $\Pi(\boldsymbol{x}|\tau)$ of molecule numbers for cells with a given age τ, and $\Pi(\tau)$ is the age distribution given by $\Pi(\tau) \propto \int_0^\tau \mathrm{d}s\, e^{\lambda(s-\tau)}\nu(s)$. The age distribution is consistent with the age-structured models of McKendrick and von Foerster [34]. In their model, the interdivision time distribution ν affecting cell age and division and determining the population growth λ are typically assumed to be fixed parameters or provided by experimental data. However, the (conditional) snapshot distribution is less studied, and, as we will see, interdivision time distribution generally depends on the gene network dynamics in the presence of selection.

We derived the first passage distribution for a cell to divide at state $\boldsymbol{x}$ and age τ, henceforth called the division distribution for brevity, follows

$$\nu(\boldsymbol{x}, \tau) = m e^{-\lambda\tau} e^{-\int_0^\tau \mathrm{d}s\gamma(s)} \gamma(\boldsymbol{x}, \tau)\Pi(\boldsymbol{x}|\tau). \tag{1a}$$

The snapshot distribution $\Pi(\boldsymbol{x}|\tau)$ of gene expression satisfies a master equation

$$\left(\frac{\partial}{\partial\tau} + \gamma(\boldsymbol{x}, \tau) - \gamma(\tau)\right)\Pi(\boldsymbol{x}|\tau) = \mathbb{Q}\Pi(\boldsymbol{x}|\tau), \tag{1b}$$

which has to be solved along with a boundary condition that connects the molecule numbers at cell birth and division:

$$\Pi(\boldsymbol{x}|0) = m\int_0^\infty \mathrm{d}\tau \sum_{\boldsymbol{x}'\in\mathcal{S}} K(\boldsymbol{x}|\boldsymbol{x}')\nu(\boldsymbol{x}', \tau). \tag{1c}$$

Here, m is the number of offspring at cell division, $\mathbb{Q}$ is the generator of the chemical master equation of the internal stochastic reaction dynamics and $\gamma(\tau) = \mathbb{E}_{\Pi(\boldsymbol{x}|\tau)}[\gamma(\boldsymbol{x}, \tau)]$ is the marginal division rate with respect to the conditional distribution $\Pi(\boldsymbol{x}|\tau)$. The partitioning kernel $K(\boldsymbol{x}|\boldsymbol{x}') = \frac{1}{2}K_1(\boldsymbol{x}|\boldsymbol{x}') + \frac{1}{2}K_1(\boldsymbol{x}' - \boldsymbol{x}|\boldsymbol{x}')$ where $K_1(\boldsymbol{x}|\boldsymbol{x}')$ and $K_1(\boldsymbol{x}' - \boldsymbol{x}|\boldsymbol{x}')$ are the marginal distributions of molecules inherited by the two daughter cells from the mother cell with intracellular state $\boldsymbol{x}'$.

The theory highlights the intricate feedback that exists between gene expression and cell division and underlies division-rate selection. The division rate multiplies the gene expression distribution in the division distribution (1a), meaning that cells where $\gamma(\boldsymbol{x}, \tau)$ is low are under-represented while cells with high division rate are

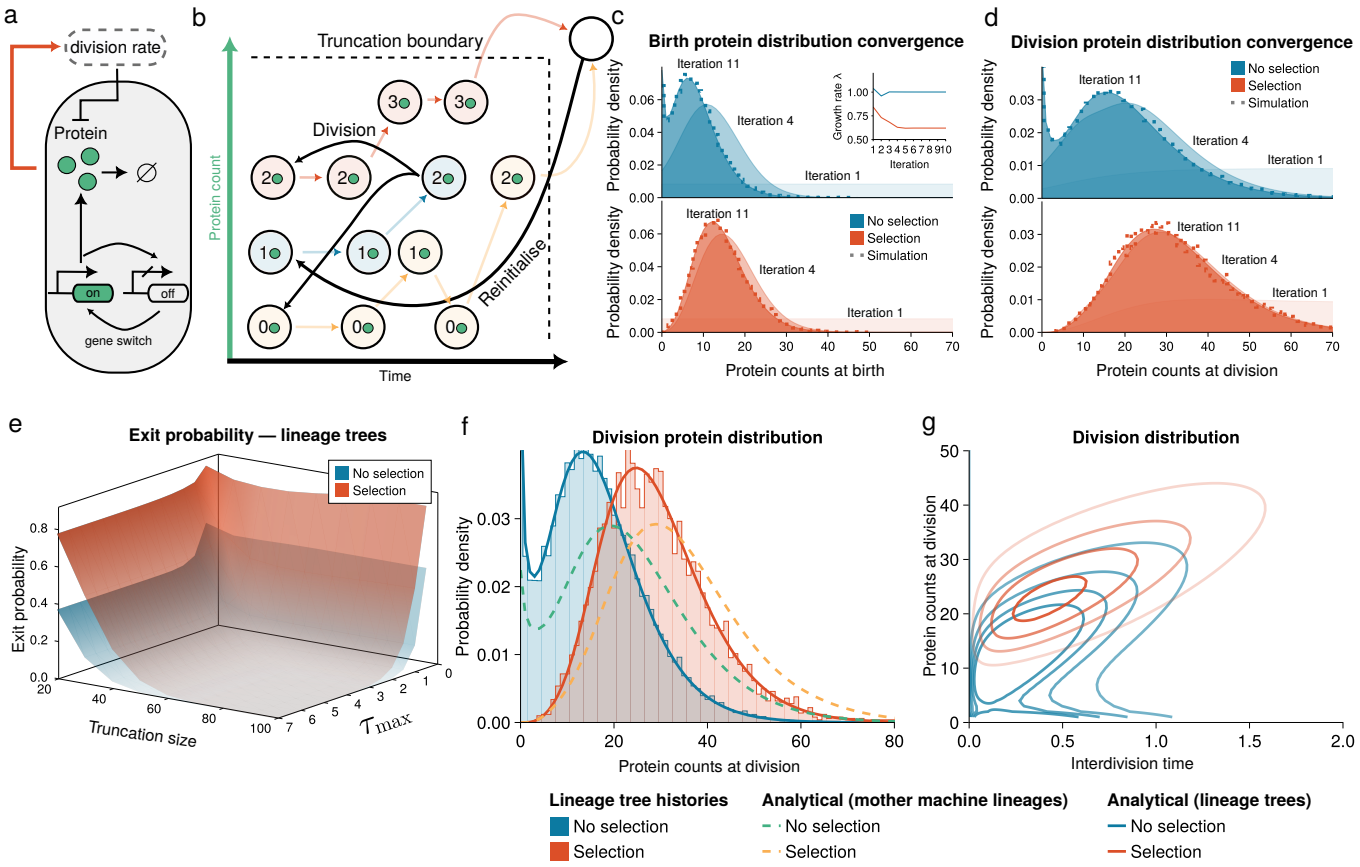

FIG. 2. **Finite state projection enables accurate prediction of selection on gene expression noise. (a)** Schematic illustration of the agent-based model. Intracellular dynamics of stochastic gene expression are modelled by the telegraph model for bursty expression of a protein. The selection effect is introduced through a division rate increasing with expression (details in SI Section S3). **(b)** Illustration of the FSP algorithm. Intuitively, gene expression (light arrows) drives cells to either commit to division or cross the truncation boundary, leading to their states being reinitialised (bold arrows). **(c-d)** Birth and division distributions for the model converge in a few iterations and agree with agent-based simulation of lineage trees obtained using the First-Division Algortihm (Methods F, see SI Figure S1 for mother machine lineages). **(e)** The exit probability due to FSP truncation decreases with truncation size and time horizon $\tau_{\max}$. **(f)** Summary distributions without (blue solid line) and with selection (red solid line) are compared to direct simulations of the lineage trees (shaded areas) are in agreement with our method. Distributions obtained using mother machine lineages (dashed) are also shown. **(g)** FSP solution of the agent-based model predicts bimodal division distribution without division-rate selection (blue lines correspond to levels of equal probability) and an unimodal division distribution in the presence of division-rate selection.

over-represented. The division distribution then determines the distribution at cell birth (1c) and the time-evolution of the gene expression distribution (1b). The latter differs from chemical master equation models as the frequency of gene expression phenotypes is not only determined by biochemical reactions but modulated by division-rate selection throughout the cell cycle.

Natural selection contributes to this feedback through the exponential dependence of the division distribution on the population growth rate. Cells dividing slower than the population doubling time are under-represented in the division distribution compared to cells that divide faster. The strength of natural selection is controlled through the average number of offspring at cell division. For example, for a lineage tree of cellular agents, we have $m = 2$ and the population growth rate λ needs to be computed self-consistently through normalising (1a) while in the mother machine setting, i.e., considering an isolated cell lineage, we have $m = 1$ and $\lambda = 0$. The difference between mother machine lineages and lineage trees provides a measure of natural selection [35, 36].

B. Division-rate vs natural selection in the telegraph gene expression model

To study selection effects, we consider the telegraph model (Figure 2a), which considers a promoter which switches between active and inactive states. Once the promoter is activated, a protein is produced in random

bursts. Selection in our model is introduced through the division rate, which we assume to be of the form:

$$\gamma(\boldsymbol{x}, \tau) = s(\boldsymbol{x}) g(\tau), \tag{2}$$

where $s(\boldsymbol{x})$ describes the effects of selection on gene expression levels $\boldsymbol{x}$ and $g(\tau)$ is the division rate in the absence of selection. Our main equations (1) cannot be solved in closed form because they are essentially an infinite system of coupled integro-ODEs. An analytical solution is only known in the special case with deterministic divisions and without selection [19, 37, 38].

To overcome this challenge, we developed a powerful approximation based on the finite state projection (FSP) method (Figure 2b, [39]). In brief, the method consists of restricting the dynamics to a finite subset of the state space $\mathcal{X} \subset \mathcal{S}$ for $\boldsymbol{x}$ and solving the dynamics of Equations (1) up to a finite cell age $\tau_{\max}$. This is akin to what is done in the standard FSP method but, in addition, we introduce (i) cell division events that split the dividing cell via binomial partitioning of molecules leading to m newborn cells and (ii) events that reinitialise single-cell trajectories once they leave the prescribed state space (Figure 2b).

We computed birth and division distributions for a fixed truncation size (Figure 2c,d) along with the corresponding growth rate (Figure 2c inset). We observe that the iterative scheme converges (Figure 2c,d) and the method allows us to compute the exit probability that arises from state space- and cell age truncation ((M1), Figure 2e). Equation (M5) corresponds to an Euler-Lotka equation of population dynamics [40] up to an error term that involves the exit probability. The exit probability measures the proportion of cells that reach division instead of being reinitialised. It decreases monotonically with maximum age $\tau_{\max}$ and truncation size (Figure 2e) guiding the accuracy of the approximation. The resulting FSP solution (Figure 2c-d shaded area) also agrees well with simulations using the FDA (dots, Methods F).

Interestingly, our analysis predicts bimodal distributions without selection while the distributions with selection are unimodal (Figure 2f-g). To clarify whether the absence of the zero-mode is due to the slow-growing sub-population being outcompeted or due to selection on division rate, we also computed the division distributions of mother machine lineages (Figure 2f). We observe qualitatively similar division protein distributions for both population lineage trees and mother machine and division rate with natural selection in the population skewing distributions towards lower expression levels. Intuitively, this can be understood through Equation (1a), which is proportional to the division rate while division times longer than the population doubling time are exponentially suppressed. Importantly, division-rate selection accounts for the absence of the slow subpopulation in both measures. This highlights that selection in the telegraph model is primarily driven by division rate.

C. Growth feedback reinforces lineage decisions in multi-stable gene regulatory networks

We wondered whether simple patterns of selection are important for cell fate decisions. Traditionally, cell differentiation is associated with multi-stability in gene regulatory networks shaping Waddington landscapes [41]. We therefore considered that positive feedback loops are commonly associated with bistability (Figure 3a). In the model without selection, a protein is expressed from a promoter which in turn increases its own expression. The production rate is modelled as a Hill function $f(x) = \frac{x^2}{K^2+x^2}$ creating a positive feedback loop. Simulation of population lineage tree histories (a random lineage of a lineage tree [35]) and a mother cell lineage reveal slow switching between the high and low protein levels (Figure 3b).

This phenomenon can be understood using effective dilution models (EDM) [1]. These effective reaction networks add one dilution reaction per species to the reaction network and can be simulated easily using ODEs or Gillespie simulations. Our analysis of the ODE model of the network reveals the S-shaped multistable response to changes in the basal transcription rates (Figure 3c, dashed yellow). Characteristically, traces simulated through the Gillespie simulations switch between two equilibria of high and slow gene expression that correspond to modes in the stationary probability distributions (Figure 3c, solid blue). Both the lineage tree and mother machine lineages show bimodal marginal snapshot distributions (Figure 3c) and thus qualitatively agree with the EDM. However, a quantitative comparison of the marginal snapshot distributions reveals different noise characteristics. EDM gives a better approximation to the mother machine lineage formulation than the lineage trees but underestimates the noise since it provides only an effective description of cell divisions (Figure 3d). We observed a similar dependence in the birth and division distributions (SI Figure S2).

Due to the presence of random switching, differentiation of this circuit can only be achieved when an external parameter is varied. Yet, how to design circuits that differentiate irreversibly in the absence of fine-tuned signals remains unclear. To this end, we study an alternative circuit where positive feedback is introduced via division rate (Figure 3e). We consider a protein is produced and degraded with a constant rate whose expression represses cell division through the Hill-type selection function $s(x) = \frac{K^2}{K^2+x^2}$. Using agent-based stochastic simulations, we observe switching between high and low expression level states at a timescale much slower than the individual cell divisions (Figure 3). The EDM displays a similar S-shaped induction curve, which corresponds well with Gillespie simulations (Figure 3g).

Comparing the distribution modes of the agent-based formulations, we find discrepancies between the predictions of the lineage tree and mother machine lineage solutions (Figure 3g, SI Figure S3). These appear in parame-

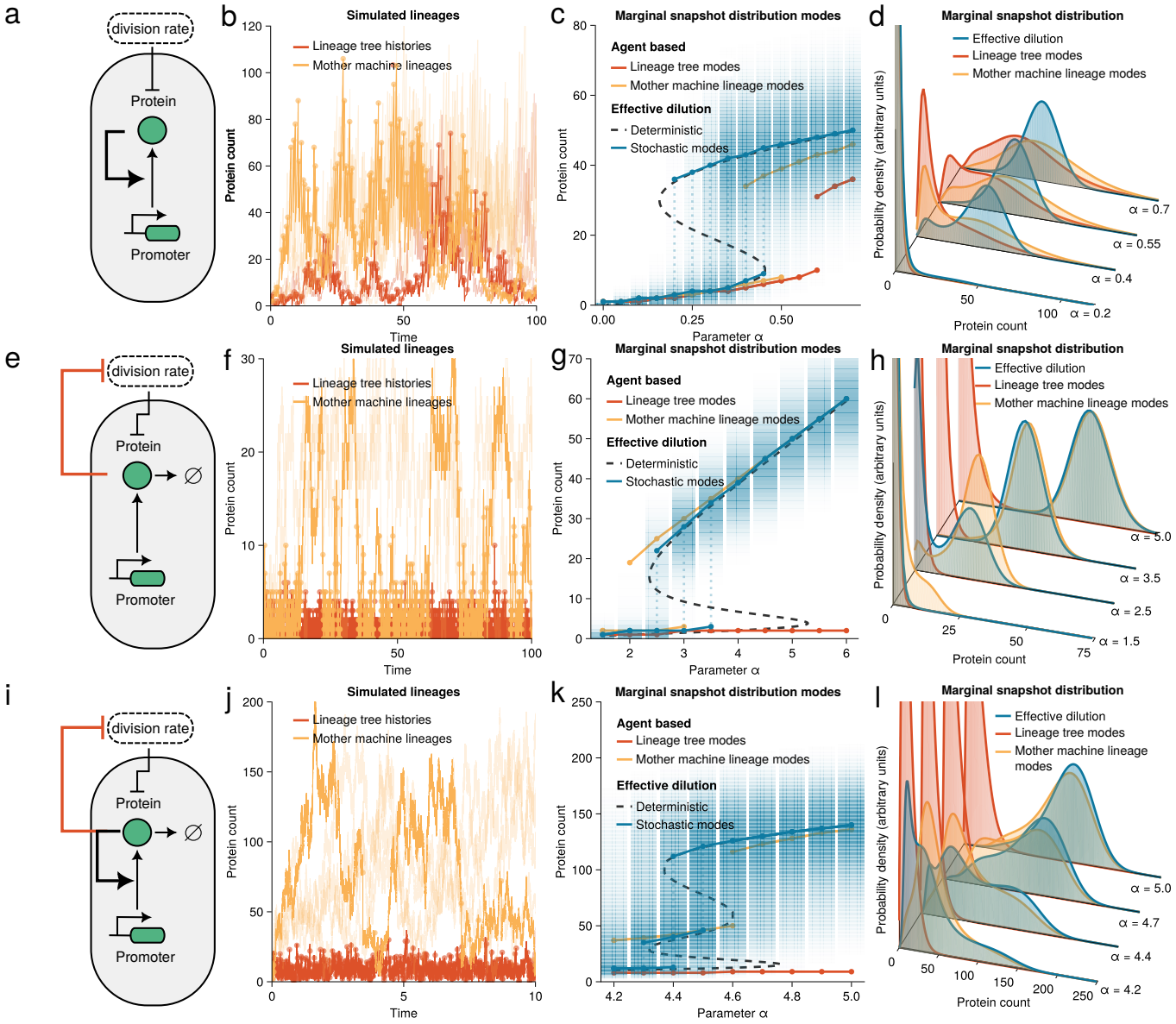

FIG. 3. **Selection reinforces lineage decisions in cellular switches. (a-d)** Agent-based model of transcriptional feedback (SI Section S4 A). **(a)** Illustration of the transcriptional feedback model where protein expression promotes its own production with parameter α corresponding to a basal synthesis rate. **(b)** Agent-based simulations of lineage tree histories and mother machine lineages ($\alpha = 0.4$) obtained using the First-Division Algorithm (Methods F) display switching between low and high protein expression states. **(c)** FSP solutions of the agent-based model predict bimodal distributions of mother machine (yellow) and lineage trees (red) over intermediate basal production rates. The EDM (black and blue) agrees well with the mother machine solution. **(d)** FSP solutions show a transition from unimodal to bimodal distributions. **(e-h)** Agent-based model with growth feedback (SI Section S4 B). **(e)** Illustration of the growth feedback model where stable proteins are synthesized with rate α and high protein abundance inhibits cell divisions. **(f)** Agent-based simulations of mother machine lineages ($\alpha = 2.0$) show switching between low and high protein levels while, in lineage tree histories, the fast dividing lineages determine the cell fate. **(g)** Protein distribution modes display bimodality for mother machine lineages and EDM but only one mode for lineage trees. **(h)** Protein distribution of mother machine lineages display slowly diving subpopulations not seen in lineage trees. **(i-l)** Agent-based model with transcriptional and growth feedback (SI Section S4 C) where protein synthesis inhibits division rate and promotes its own production rate. EDM and mother machine lineages have three stable modes while lineage trees show that fast-dividing cell lineages take over the population.

ter regimes where the EDM predicts bimodality (dashed black and solid blue lines). The prediction of the mother machine lineage follows the EDM qualitatively but shows a different transition point, where the expression switches from low to high expression (Figure 3h). This demonstrates that division rate can drive bimodality in growing

cells via division-rate selection.

The agent-based model predicts a single subpopulation with repressed protein expression in the marginal snapshot distribution over lineage trees (Figure 3g, red line). This is in stark contrast to the bimodality of mother machine lineages and EDM that prefer the slow-dividing cells (Figure 3h, red line). This constitutes the breakdown of the EDM to describe population-level lineage decisions. Thus the coupling of division-rate selection and natural selection selects only the fastest growing population. This shows that population dynamics can contribute to enforcing lineage decisions through natural selection.

We asked if selection could provide a general mechanism for lineage decisions. We therefore combine the positive feedback that exists between expression and growth into a single model. In the EDM, such a circuit predicts three or two stable points depending on the parameter regime (Figure 3k). Simulations of mother machine lineages show switching between the tree expression levels with very slow cell divisions in the highly expressed states (Figure 3j, orange line). In stark contrast, the histories of population lineage trees display fast divisions selecting only a single lowly expressed (Figure 3j, red line) as expected due to the negative feedback between expression and division rate. The higher expression level states in a population lineage tree get rapidly outcompeted by fast dividing cells. Comparing the distribution modes of the different measures, we observe that the EDM model explores all three states (Figure 3k-l, SI Figure S4). The mother machine lineages mostly explore the two high expression states corresponding to slow-dividing cells while the population lineage trees display exclusively the lowly expressed state that promotes fast cell proliferation. The coupling between gene expression and growth thus represents a robust strategy to implement cell fate decisions in populations.

D. Model-based inference predicts DNA damage response from division-rate selection

We now apply our modelling framework to understand how cells respond to stress. To this end, we investigate the activity of the SOS pathway quantified using the SOS promoter *PsulA* driving the expression of a fluorescent reporter [42]. Surprisingly, we found that the expression of this pathway is highly heterogeneous even in unstressed conditions (Figure 4c, shaded red bars) and is well fit by a bursty gene expression model (Figure 4a).

In the model, we assumed the division rate to be of the form (2), where $s(\boldsymbol{x})$ models a damage-induced modulation and $g(\tau)$ is the division rate in unstressed conditions. The latter can be inferred directly from the interdivision time data using a non-parametric kernel density estimator (Figure 4b, shaded red bars) and fits well the interdivision time distributions. To infer the reaction kinetics in unstressed conditions, we convert fluorescence measurements to molecule numbers (SI Figure S6) and define a likelihood function via the division distribution $\nu(\boldsymbol{x}, \tau)$ that can be maximised using Bayesian optimisation (Methods H, [43]) to fit the reaction parameters, i.e., burst size and burst frequency.

When DNA damage was induced, cells displayed a long tail of slowly dividing cells and increased levels of SOS pathway expression (Figure 4b,c shaded blue). Intuitively, this could suggest upregulation of the SOS pathway as a stress response but also positive selection on SOS levels. We investigated this by inferring stress-induced selection function $s(x)$ (Figure 4b inset, see SI Section S5 B), but kept the reaction parameters as in unstressed conditions, which provided good agreement with the data (Figure 4b,c solid blue). We hence conclude that upregulation of SOS expression is not required to fit the data. We wondered whether these effects could equally be explained through a neutral model without selection but with different interdivision time distributions. The latter gave a worse fit as it overestimated the protein-age correlation at division (SI Figure S7).

Our findings thus suggest that the DNA damage response is driven solely by division-rate selection in this system. The observation alludes to a possible bet-hedging strategy in *Escherichia coli* where SOS expression is heterogeneous in unstressed conditions to better deal with environmental changes in stress levels [44].

E. Antibiotic-resistance gene expression involves division-rate-selection and adaptation

As a second application, we considered time-lapse data of *Escherichia coli* expressing an antibiotic resistance gene $\mathrm{Sm^R}$, an efflux pump conferring resistance to *streptomycin* [35]. Again, we find that protein distributions are highly heterogeneous even in the absence of antibiotics and can also be fit by a bursty gene expression model (Figure 4e,f,g solid red) parametrised through burst size and burst frequency.

We wondered whether antibiotic resistance gene expression represents a possible bet-hedging strategy similar to one observed for the SOS response (Figure 4a-d). To this end, we again modelled the division rate via (2), where now $g(\tau)$ is the division rate in the absence of antibiotics and $s(\boldsymbol{x})$ is a drug-induced modulation of division rate. We converted fluorescence to molecule numbers (SI Figure S8) and used Bayesian optimisation to fit the protein-dependent modulation of the division rate $s(\boldsymbol{x})$ underlying the interdivision time and protein distributions under conditions where cells have been exposed to sub-lethal doses of antibiotics. While this division rate described well the reduction in protein expression (Figure 4g dashed blue), it failed to account for the increase in interdivision time (Figure 4f dashed blue). Similarly, considering a model with no selection but matched interdivision time distributions did not fit the protein expression data (SI Figure S9). Intuitively, the data suggested

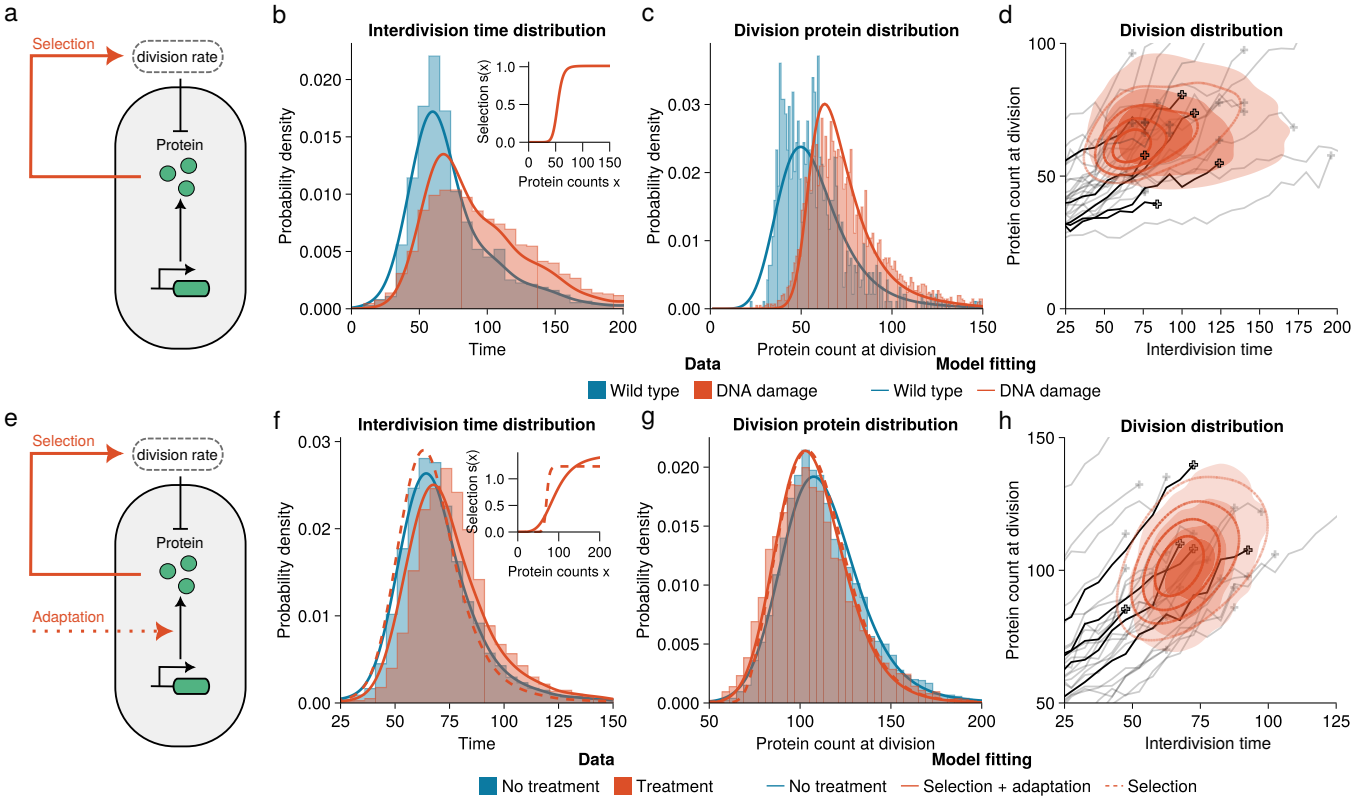

FIG. 4. **Inference of selection effects in *Escherichia coli* cells. (a)** Agent-based model of the SOS response involves a bursty gene expression model with an age-dependent division rate. DNA damage is induced through a gene expression-dependent modulation of the division rate. **(b-c)** Interdivision time and protein distributions from the mother machine lineages (fluorescent reporter, medium growth conditions [42]) in unstressed (blue areas) and damage-induced mother machine lineages (red area) are well fit by the agent-based model ($m = 1$, see SI Section S5 B for fit parameters). The inset shows the selection function $s(x)$ obtained in damage-induced conditions. **(d)** The division distribution of the fitted model shows a distinctly peaked distribution (red lines) that compares well with the experimental distribution (shaded red area) and single-cell traces of the data (representative traces shown in black and grey). **(e)** Agent-based model of antibiotic resistance gene expression using a bursty gene expression model with age-dependent division rate. Antibiotic treatment response involves positive feedback of protein expression and division through a gene expression-dependent division rate and adaption of gene expression parameters. **(f-g)** Statistics of the division distribution of the lineage trees (fluorescent fusion-protein genome-integrated reporter, [35]) in untreated (blue area) and antibiotic-treated cells (red area). Lineage tree data is well fitted by the agent-based model combining drug-dependent selection and adaptation (solid red line), but not using selection alone (dashed red line, $m = 2$, parameters in SI Section S5 C). The inset shows the corresponding selection functions $s(x)$ obtained in treated conditions. **(h)** The division distribution under treatment shows a peaked distribution (red lines) that compares well with the experimental distribution and single-cell traces of the data (representative traces shown in black and grey).

attenuated protein expression while cells divided slightly slower (Figure 4f,g blue area), which is inconsistent with the division-selection model.

We thus hypothesised that cells adapt gene expression during treatment. Indeed, allowing the combined effects of selection on the protein as well as refitting the rate parameters between the conditions provides good agreement with the experimental data of interdivision time (solid blue in Figure 4f), division protein (solid blue in Figure 4g) as well as the joint division distribution of protein count and interdivision time (solid blue in Figure 4h). Our analysis suggests that cells increase burst size during the drug response (burst size increased from 1.4 to 2.1, SI Section S5 C), and that adaption plays a role in the drug response in *Escherichia coli*.

DISCUSSION

We developed a novel agent-based framework for quantifying the feedback between stochastic gene expression, cell division and population dynamics. Our approach allows us to derive the division distributions of lineage trees directly accessible in live-cell imaging of growing cell populations. These distributions are generally distinct from the first-passage distributions of the conventional chemical master equation due to the effects of division rate, natural selection, and cell history. Our findings thus provide a quantitative understanding of how natural selection and division rates shape phenotypes and allow decision-making in response to gene expression.

Our method enables accurate solutions of agent-based models and efficient parameter inference. Previous approaches typically relied on costly agent-based simulations [45]. To this end, we proposed a finite state projection solution. We identified the exit probability of crossing the state space, which serves as an error gauge and quality assurance of the numerical scheme resulting from truncating the state space and setting a finite maximum age for cells. However, the FSP method presents (like the master equation) a large system of coupled differential equations. Tensor-train methods and clever state space truncations have alleviated some of these challenges [46].

Multi-stable gene regulatory networks are fundamental in development, triggering cellular responses and cell fate decisions. Naturally, these networks require environmental signals for robust decision-making, while otherwise, they are subject to continuing fluctuations that can lead to reversible phenotypic switching. Our methodology allowed us to understand several models implementing positive feedback between protein expression and division rate. We showed that positive feedback coupled with population dynamics leads to phenotypic switching of mother machine lineages but not in the histories of lineage trees, demonstrating that mother machine lineages generally do not represent typical cell lineages. This observation holds over long timescales when mother machine lineages and lineage tree histories, originating from the same ancestral cell, switch initially but gradually diverge over time (SI Figure S5). Intuitively, the mother machine samples lineages with a probability that decreases exponentially with the number of divisions, thus oversampling slowly dividing cells compared to lineage trees [35]. Importantly, division-rate selection presents a robust mechanism of irreversible lineage choice in a population. This mechanism requires slow-cycling progenitor cells as observed in stem cell lineages [7, 47, 48].

The present framework provides multiple advantages over previously proposed stochastic modelling approaches for single-cell data. Importantly, our framework revealed irreversible cell fate decisions that cannot be captured using traditional chemical master equation models. The agent-based approach goes beyond the snapshot statistics because it explicitly accounts for age structure. This allows us to assess lineage statistics and dynamics, such as cell birth, division events, or certain cell cycle stages. As we have demonstrated, this information is readily available from time-lapse data and allows for parameter fitting and model selection. Although we focused on cell age, our framework extends to cell size control, which could provide further data insights.

Our agent-based theory provides new insights into how cells respond to stress and drugs based on gene expression and division feedback. To this end, we employed Bayesian optimisation for parameter inference on two single-cell datasets in *Escherichia coli* [35, 42]. The framework allowed us to efficiently integrate data from multiple conditions to identify selection effects and evaluate competing model hypotheses. Our stochastic model suggested the increase in SOS pathway expression in response to induced DNA damage [42] does not require upregulation of SOS expression but is achieved effectively through division-rate selection. This suggests that heterogeneous SOS expression in unstressed conditions could provide a bet-hedging strategy. A similar model applied to the response of an antibiotic resistance gene revealed that division-rate selection alone was not sufficient to explain the data but that cells adapt their gene expression during treatment.

Crucially, our analysis quantified changes in gene expression and interdivision times between different experimental conditions. Yet, we cannot exclude that selection effects are present even in supposedly neutral conditions. It remains to be seen whether differences between division rate and natural selection can be quantified from time-lapse observations of individual lineage trees. For simplicity, we assumed a multiplicative selection model, Equation (2), where gene expression-dependent effects act independently from other sources effectively modelled through cell age. Studying the effects of cell-cycle-dependent feedback on selection would be an interesting avenue for future research.

Our new theory enables us to understand how variability in gene expression shapes phenotypes and propagates to population dynamics. We used the method to uncover mechanisms of cell fate decision-making, study how cells respond to stress, and adapt their gene expression programmes in response to drugs. Our findings thus significantly advance the understanding of how cells make decisions through coupling gene networks with growth and division. We expect our methods to provide insights into the role of heterogeneity in growth-associated disease and drug resistance, such as in cancer [49].

FUNDING

UKRI supported this work through a Future Leaders Fellowship (MR/T018429/1 to PT).

METHODS

F. First division algorithm for exact agent-based simulation

We present an exact simulation algorithm to the agent-based model of cells in a growing population from time t_0 to T. This is an extended version of the First Division Algorithm [21] and the Extrande thinning method for sampling division times [50]. The algorithm uses a lookup horizon Δt over which the division rate can be bounded.

1. *Initialisation.* Initialise the cell population at time $t = t_0$ by assigning each cell i an age $\tau_i(t)$ at time t and molecule count vector $\boldsymbol{x}_i(\tau_i(t))$.

2. *Intra-cellular reaction dynamics.* For each cell i simulate the trajectory of molecule counts in the age interval $[\tau_i(t), \tau_i(t+\Delta t)]$ using the Gillespie algorithm.

3. *Cell division times.* For each cell i sample the division time $t_{d,i}$ via the *thinning method.*

   (a) Compute an upper bound of the division rate by $\gamma_{max} \geq \gamma(\boldsymbol{x}(\tau(t)), \tau(t))$ for all t in $[t, t+\Delta t]$.

   (b) Sample an event time t^* from exponential distribution with rate γ_{max}. The proposed division time is then $t_p = t + t^*$.

   - If $t_p > t + \Delta t$ then reject the proposed division time t_p and conclude that the cell does not divide in this time interval.
   - If $t_p \leq t + \Delta t$, sample a u from uniform distribution on the interval $[0, 1]$ and consider two options. Accept the proposed time t_p as the next division time for the cell if $\frac{\gamma(\boldsymbol{x}(\tau(t_p),\tau(t_p))}{\gamma_{max}} \leq u$. Otherwise, set $t = t_p$ and repeat from step 3b.

4. *Next division time.* Determine the next cell to divide by $j = \text{argmin}_i t_{d,i}$.

5. *Cell division.* Replace the dividing cell j by two daughter cells at age 0. Set the molecule counts of one by sampling from the partitioning distribution $K_1(\boldsymbol{x}|\boldsymbol{x}_j(\tau(t_{d,j})))$ and give the remaining molecules to the other daughter. Simulate the intracellular reaction dynamics of the two daughter cells for the time interval $[t_{d,j}, t+\Delta t]$ and sample their division times as in Step 3.

6. Repeat the Steps 4-5 till no more divisions occur in the time interval $[t, t+\Delta t]$. Set $t = t + \Delta t$ and $\boldsymbol{x}_i$ to the molecule counts of cell i at time t. If $t \geq T$ stop, else go to Step 2.

G. Finite state projection-based solution to the agent-based model

We developed the FSP scheme for growing cell populations. FSP relies on considering the dynamics over a finite truncated state space $\mathcal{X} \subset \mathcal{S}$ for $\boldsymbol{x}$. The scheme effectively computes $\Pi'_n(\boldsymbol{x}|\tau) = \Pi_n(\boldsymbol{x}|\tau)e^{-\int_0^\tau \mathrm{d}s\gamma(s)}$, the product of the probability that cells have $\boldsymbol{x}$ molecules when they reach age τ and the probability that cells have not yet divided at that age. The cells that leave the truncated state space or do not divide in the age interval $[0, \tau_{\max}]$ are reinitialised at age 0 according to the division kernel $K(\boldsymbol{x}|\boldsymbol{x}')$. The corresponding exit probability to be reinitialised is given by

$$\varepsilon_n(\boldsymbol{x}, \lambda_n) = \int_0^{\tau_{\max}} \mathrm{d}\tau \bar{q}(\boldsymbol{x})\Pi'_n(\boldsymbol{x}|\tau)e^{-\lambda_n\tau} + e^{-\lambda_n\tau_{\max}}\Pi'_n(\boldsymbol{x}|\tau_{\max}), \quad \text{(M1)}$$

which can be self-consistently computed along with the FSP approximation. $\bar{q}(\boldsymbol{x})$ is the rate a which cells with intracellular state $\boldsymbol{x}$ leave the truncated state space. That is, we define $\bar{q}(\boldsymbol{x}) = \sum_{\bar{\boldsymbol{x}}\in\bar{\mathcal{X}}} q(\bar{\boldsymbol{x}}, \boldsymbol{x})$ where $q(\boldsymbol{x}', \boldsymbol{x})$ are rates for the exponentially distributed time it takes for a cell to transition from intracellular state $\boldsymbol{x}$ to state $\boldsymbol{x}'$ and the complement $\bar{\mathcal{X}} = \mathcal{S} \setminus \mathcal{X}$ are the intracellular states outside truncation boundary. The first term of (M1) corresponds to the probability mass leaving the population though the FSP boundary states into the complement $\bar{\mathcal{X}}$ and the probability mass of cells that do not divide in the interval $[0, \tau_{\max}]$. The algorithm is as follows:

1. Set $n = 0$ and provide an initial guess for the birth distribution $\Pi'_0(\boldsymbol{x}|0)$ and growth rate λ_0.

2. Solve

$$\frac{\partial}{\partial\tau}\Pi'_n(\boldsymbol{x}|\tau) = (\mathbb{Q}_{\mathcal{X}} - \gamma(\boldsymbol{x}, \tau))\,\Pi'_n(\boldsymbol{x}|\tau). \quad \text{(M2)}$$

   for all $\boldsymbol{x}$ in $\mathcal{X}$ where $\mathbb{Q}_{\mathcal{X}}$ is defined as

$$\mathbb{Q}_{\mathcal{X}}\Pi'_n(\boldsymbol{x}|\tau) = \sum_{\boldsymbol{x}'\in\mathcal{X}} q(\boldsymbol{x}, \boldsymbol{x}')\Pi'_n(\boldsymbol{x}'|\tau) - q(\boldsymbol{x}', \boldsymbol{x})\Pi'_n(\boldsymbol{x}|\tau). \quad \text{(M3)}$$

3. Solve

$$\nu_n(\boldsymbol{x}, \tau) = me^{-\lambda_n\tau}\gamma(\boldsymbol{x}, \tau)\Pi'_n(\boldsymbol{x}|\tau), \quad \text{(M4)}$$

$$1 - \sum_{\boldsymbol{x}\in\mathcal{X}} \varepsilon_n(\boldsymbol{x}, \lambda_n) = \int_0^{\tau_{\max}} \mathrm{d}\tau \sum_{\boldsymbol{x}\in\mathcal{X}} \nu_n(\boldsymbol{x}, \tau). \quad \text{(M5)}$$

   to obtain the growth rate λ_n and the division distribution $\nu_n(\boldsymbol{x}, \tau)$

4. Update the boundary condition $\Pi_{n+1}(\boldsymbol{x}|0)$ using

$$\Pi_{n+1}(\boldsymbol{x}|0) = \sum_{\boldsymbol{x}'\in\mathcal{X}} K(\boldsymbol{x}|\boldsymbol{x}')\left[\int_0^\infty \mathrm{d}\tau\nu_n(\boldsymbol{x}', \tau) + \varepsilon(\boldsymbol{x}', \lambda_n)\right], \quad \text{(M6)}$$

5. Repeat from 2. until λ_n and $\Pi_n(\boldsymbol{x}|0)$ converge.

For mother machine lineages, we have $m = 1$ and the population stays constant and hence $\lambda_n = 0$ for all n. In this case only the initial condition $\Pi_n(\boldsymbol{x}|0)$ is iterated. The details of the derivation are given in SI Section S2.

H. Inference from single-cell data

To perform parameter fitting for the agent-based models we defined a likelihood based on N independent observations of the division distribution $\nu(\boldsymbol{x}, \tau)$ as

$$\log \mathcal{L}(\boldsymbol{\theta}) = \sum_{i=1}^{N} \left(\nu(x_i, \tau_i; \boldsymbol{\theta}) + \sum_{j=1}^{m} K(x_{i,j} | x_i; \boldsymbol{\theta}) \right), \quad \text{(M7)}$$

where $(x_i, \{x_{i,j}\}_{j=1}^{m}, \tau_i)_{i=1,..,N}$ are the observations of protein counts of mother cell at division, protein counts of the daughter cells, and interdivision times and θ is the vector of parameters of model.

Inference of reaction kinetics and division rate requires absolute quantification of protein numbers. Assuming that the partitioning of molecules between the daughter cells is binomial with parameter $\frac{1}{2}$, a linear relationship $f_i = \alpha \cdot x_i$ between fluorescence f and absolute protein number x_i can be obtained (SI Section S5 A). In practice, one fits the relation between the partitioning variance of daughter fluorescence conditional on mother fluorescence (SI Figures S6 and S8). The inference problem then becomes

$$\log \mathcal{L}(\boldsymbol{\theta}) = \sum_{i=1}^{N} \nu(f_i/\alpha, \tau_i; \boldsymbol{\theta}) \quad \text{(M8)}$$

$(f_i, \tau_i)_{i=1,..,N}$ are the measured fluorescence intensity at division and the corresponding inter-division times.

[1] H. H. McAdams and A. Arkin, Stochastic mechanisms in gene expression, Proceedings of the National Academy of Sciences **94**, 814 (1997).

[2] M. B. Elowitz, A. J. Levine, E. D. Siggia, and P. S. Swain, Stochastic gene expression in a single cell, Science **297**, 1183 (2002).

[3] J. M. Raser and E. K. O'shea, Noise in gene expression: Origins, consequences, and control, Science **309**, 2010 (2005).

[4] M. Ackermann, A functional perspective on phenotypic heterogeneity in microorganisms, Nature Reviews Microbiology **13**, 497 (2015).

[5] B. M. Martins and J. C. Locke, Microbial individuality: How single-cell heterogeneity enables population level strategies, Current opinion in microbiology **24**, 104 (2015).

[6] H. Y. Kueh, A. Champhekar, S. L. Nutt, M. B. Elowitz, and E. V. Rothenberg, Positive feedback between PU. 1 and the cell cycle controls myeloid differentiation, Science **341**, 670 (2013).

[7] S. Furutachi, H. Miya, T. Watanabe, H. Kawai, N. Yamasaki, Y. Harada, I. Imayoshi, M. Nelson, K. I. Nakayama, Y. Hirabayashi, *et al.*, Slowly dividing neural progenitors are an embryonic origin of adult neural stem cells, Nature neuroscience **18**, 657 (2015).

[8] A. R. Barr, S. Cooper, F. S. Heldt, F. Butera, H. Stoy, J. Mansfeld, B. Novák, and C. Bakal, DNA damage during S-phase mediates the proliferation-quiescence decision in the subsequent G1 via p21 expression, Nature communications **8**, 14728 (2017).

[9] O. Patange, C. Schwall, M. Jones, C. Villava, D. A. Griffith, A. Phillips, and J. C. Locke, Escherichia coli can survive stress by noisy growth modulation, Nature communications **9**, 5333 (2018).

[10] N. M. Sampaio, C. M. Blassick, V. Andreani, J.-B. Lugagne, and M. J. Dunlop, Dynamic gene expression and growth underlie cell-to-cell heterogeneity in Escherichia coli stress response, Proceedings of the National Academy of Sciences **119**, e2115032119 (2022).

[11] N. Q. Balaban, J. Merrin, R. Chait, L. Kowalik, and S. Leibler, Bacterial Persistence as a Phenotypic Switch, Science **305**, 1622 (2004).

[12] Y. Wakamoto, N. Dhar, R. Chait, K. Schneider, F. Signorino-Gelo, S. Leibler, and J. D. McKinney, Dynamic persistence of antibiotic-stressed mycobacteria, Science **339**, 91 (2013).

[13] L. Gerosa, C. Chidley, F. Fröhlich, G. Sanchez, S. K. Lim, J. Muhlich, J.-Y. Chen, S. Vallabhaneni, G. J. Baker, D. Schapiro, *et al.*, Receptor-driven ERK pulses reconfigure MAPK signaling and enable persistence of drug-adapted BRAF-mutant melanoma cells, Cell systems **11**, 478 (2020).

[14] C. Tan, P. Marguet, and L. You, Emergent bistability by a growth-modulating positive feedback circuit, Nature chemical biology **5**, 842 (2009).

[15] A. Y. Weiße, D. A. Oyarzún, V. Danos, and P. S. Swain, Mechanistic links between cellular trade-offs, gene expression, and growth, Proceedings of the National Academy of Sciences **112**, E1038 (2015).

[16] C. Aditya, F. Bertaux, G. Batt, and J. Ruess, Using single-cell models to predict the functionality of synthetic circuits at the population scale, Proceedings of the National Academy of Sciences **119**, e2114438119 (2022).

[17] P. S. Swain, M. B. Elowitz, and E. D. Siggia, Intrinsic and extrinsic contributions to stochasticity in gene expression, Proceedings of the National Academy of Sciences **99**, 12795 (2002).

[18] D. Huh and J. Paulsson, Non-genetic heterogeneity from stochastic partitioning at cell division, Nature genetics **43**, 95 (2011).

[19] Z. Cao and R. Grima, Analytical distributions for detailed models of stochastic gene expression in eukaryotic cells, Proceedings of the National Academy of Sciences **117**, 4682 (2020).

[20] M. Hashimoto, T. Nozoe, H. Nakaoka, R. Okura, S. Akiyoshi, K. Kaneko, E. Kussell, and Y. Wakamoto, Noise-driven growth rate gain in clonal cellular populations, Proceedings of the National Academy of Sciences **113**, 3251 (2016).

[21] P. Thomas, Making sense of snapshot data: Ergodic principle for clonal cell populations, Journal of The Royal Society Interface **14**, 20170467 (2017).

[22] P. Thomas, Intrinsic and extrinsic noise of gene expression in lineage trees, Scientific Reports **9**, 474 (2019).

[23] D. J. Kiviet, P. Nghe, N. Walker, S. Boulineau, V. Sunderlikova, and S. J. Tans, Stochasticity of metabolism

and growth at the single-cell level, Nature **514**, 376 (2014).

[24] P. Thomas, G. Terradot, V. Danos, and A. Y. Weiße, Sources, propagation and consequences of stochasticity in cellular growth, Nature communications **9**, 4528 (2018).

[25] F. A. Hughes, A. R. Barr, and P. Thomas, Patterns of interdivision time correlations reveal hidden cell cycle factors, Elife **11**, e80927 (2022).

[26] K. R. Ghusinga, C. A. Vargas-Garcia, and A. Singh, A mechanistic stochastic framework for regulating bacterial cell division, Scientific Reports **6**, 30229 (2016).

[27] J. Kuntz, P. Thomas, G.-B. Stan, and M. Barahona, The exit time finite state projection scheme: Bounding exit distributions and occupation measures of continuous-time Markov chains, SIAM Journal on Scientific Computing **41**, A748 (2019).

[28] M. Panlilio, J. Grilli, G. Tallarico, I. Iuliani, B. Sclavi, P. Cicuta, and M. Cosentino Lagomarsino, Threshold accumulation of a constitutive protein explains E. coli cell-division behavior in nutrient upshifts, Proceedings of the National Academy of Sciences **118**, e2016391118 (2021).

[29] K. Biswas and N. Brenner, Cell-division time statistics from stochastic exponential threshold-crossing, BioRxiv 10.1101/2022.08.21.504683 (2022).

[30] L. Luo, Y. Bai, and X. Fu, Stochastic threshold in cell size control, Physical Review Research **5**, 013173 (2023).

[31] T. Mora and A. M. Walczak, Effect of phenotypic selection on stochastic gene expression, The Journal of Physical chemistry B **117**, 13194 (2013).

[32] M. Ciechonska, M. Sturrock, A. Grob, G. Larrouy-Maumus, V. Shahrezaei, and M. Isalan, Emergent expression of fitness-conferring genes by phenotypic selection, PNAS nexus **1**, pgac069 (2022).

[33] P. Wang, L. Robert, J. Pelletier, W. L. Dang, F. Taddei, A. Wright, and S. Jun, Robust growth of Escherichia coli, Current biology **20**, 1099 (2010).

[34] H. Von Foerster, Some remarks on changing populations, The kinetics of cellular proliferation , 382 (1959).

[35] T. Nozoe, E. Kussell, and Y. Wakamoto, Inferring fitness landscapes and selection on phenotypic states from single-cell genealogical data, PLOS Genetics **13**, 1 (2017).

[36] S. Yamauchi, T. Nozoe, R. Okura, E. Kussell, and Y. Wakamoto, A unified framework for measuring selection on cellular lineages and traits, Elife **11**, e72299 (2022).

[37] O. G. Berg, A model for the statistical fluctuations of protein numbers in a microbial population, Journal of theoretical biology **71**, 587 (1978).

[38] I. G. Johnston and N. S. Jones, Closed-form stochastic solutions for non-equilibrium dynamics and inheritance of cellular components over many cell divisions, Proceedings of the Royal Society A: Mathematical, Physical and Engineering Sciences **471**, 20150050 (2015).

[39] B. Munsky and M. Khammash, The finite state projection algorithm for the solution of the chemical master equation, The Journal of Chemical Physics **124**, 044104 (2006).

[40] E. O. Powell, Growth Rate and Generation Time of Bacteria, with Special Reference to Continuous Culture, Microbiology **15**, 492 (1956).

[41] M. A. Coomer, L. Ham, and M. P. Stumpf, Noise distorts the epigenetic landscape and shapes cell-fate decisions, Cell Systems **13**, 83 (2022).

[42] S. Jaramillo-Riveri, J. Broughton, A. McVey, T. Pilizota, M. Scott, and M. El Karoui, Growth-dependent heterogeneity in the DNA damage response in Escherichia coli, Molecular Systems Biology **18**, e10441 (2022).

[43] B. Shahriari, K. Swersky, Z. Wang, R. P. Adams, and N. de Freitas, Taking the Human Out of the Loop: A Review of Bayesian Optimization, Proc. IEEE **104**, 148 (2016).

[44] J.-W. Veening, W. K. Smits, and O. P. Kuipers, Bistability, Epigenetics, and Bet-Hedging in Bacteria, Annual Review of Microbiology **62**, 193 (2008).

[45] A. C. S. Jørgensen, A. Ghosh, M. Sturrock, and V. Shahrezaei, Efficient Bayesian inference for stochastic agent-based models, PLoS Computational Biology **18**, e1009508 (2022).

[46] I. G. Ion, C. Wildner, D. Loukrezis, H. Koeppl, and H. De Gersem, Tensor-train approximation of the chemical master equation and its application for parameter inference, The Journal of Chemical Physics **155**, 10.1063/5.0045521 (2021).

[47] L. Liu, W. Michowski, A. Kolodziejczyk, and P. Sicinski, The cell cycle in stem cell proliferation, pluripotency and differentiation, Nature Cell Biology **21**, 1060 (2019).

[48] E. Fuchs, The Tortoise and the Hair: Slow-Cycling Cells in the Stem Cell Race, Cell **137**, 811 (2009).

[49] D. Shiokawa, H. Sakai, H. Ohata, T. Miyazaki, Y. Kanda, S. Sekine, D. Narushima, M. Hosokawa, M. Kato, Y. Suzuki, H. Takeyama, H. Kambara, H. Nakagama, and K. Okamoto, Slow-Cycling Cancer Stem Cells Regulate Progression and Chemoresistance in Colon Cancer, Cancer Research **80**, 4451 (2020).

[50] M. Voliotis, P. Thomas, R. Grima, and C. G. Bowsher, Stochastic Simulation of Biomolecular Networks in Dynamic Environments, PLOS Computational Biology **12**, e1004923 (2016)

Supplementary Information

S1. SNAPSHOT DENSITY

As done in [SI6, SI7] we derive the time-evolution of snapshot density $n(\boldsymbol{x}, \tau, t)$ corresponding to the mean number of cells with molecule counts $\boldsymbol{x}$ and age τ at time t as

$$(\partial_t + \partial_\tau + \gamma(\boldsymbol{x}, \tau))\, n(\boldsymbol{x}, \tau, t) = \mathbb{Q} n(\boldsymbol{x}, \tau, t) \tag{S1}$$

with the boundary condition

$$n(\boldsymbol{x}, 0, t) = m \int_0^\infty ds \sum_{\boldsymbol{x}' \in \mathcal{S}} dx' K(\boldsymbol{x}|\boldsymbol{x}') \gamma(\boldsymbol{x}', \tau) n(\boldsymbol{x}', \tau, t). \tag{S2}$$

The sum is taken over the countable state space $\mathcal{S}$ for the trait vector $\boldsymbol{x}$. The boundary condition corresponds to the cell divisions replacing a mother cell by m newborn daughter cells with $K(\boldsymbol{x}|\boldsymbol{x}')$ denoting the probability that a daughter cell inherits $\boldsymbol{x}$ molecules from a total of $\boldsymbol{x}'$ molecules of the mother cell. The division rate $\gamma(\boldsymbol{x}, \tau)$ depends on both the cell age as well as the cell trait vector $\boldsymbol{x}$. The traits $\boldsymbol{x}$ evolve according to a Markov jump process with generator $\mathbb{Q}$. In particular, let

$$\mathbb{Q} n(\boldsymbol{x}, \tau, t) = \sum_{\boldsymbol{x}' \in \mathcal{S}} q(\boldsymbol{x}, \boldsymbol{x}') n(\boldsymbol{x}, \tau, t) - q(\boldsymbol{x}', \boldsymbol{x}) n(\boldsymbol{x}, \tau, t) \tag{S3}$$

where $q(\boldsymbol{x}', \boldsymbol{x})$ are rates for the exponentially distributed times it takes for a cell to transition from intracellular state $\boldsymbol{x}$ to state $\boldsymbol{x}'$. Finally $m = 2$ corresponds to the population lineage trees where each division results in two offsprings while $m = 1$ corresponds to tracking a single offspring in mother machine lineages.

S2. METHOD DERIVATION

In this section we detail the construction of the finite state projection-based method for computing approximate solutions to the agent-based model. A method where approximation error resulting from the truncation of the state space of the intracellular dynamics as well as error resulting from the finite time-horizon can be tracked and controlled. To that end, consider a truncated state space $\mathcal{X} \subseteq \mathcal{S}$ for the trait $\boldsymbol{x}$ and let $\bar{\mathcal{X}}$ denote the complement of $\mathcal{X}$. The evolution equations that consider only the evolution of cells that remain within the truncated state space $\mathcal{X}$ is given by the following.

$$(\partial_t + \partial_\tau - \gamma(\boldsymbol{x}, \tau)) n(\boldsymbol{x}, \tau, t) = \sum_{\boldsymbol{x}' \in \mathcal{X}} q(\boldsymbol{x}, \boldsymbol{x}') n(\boldsymbol{x}', \tau, t) - q(\boldsymbol{x}', \boldsymbol{x}) n(\boldsymbol{x}, \tau, t) \tag{S4}$$

$$n(\boldsymbol{x}', 0, t) = m \int d\tau \sum_{\boldsymbol{x}' \in \mathcal{X}} K(\boldsymbol{x}'|\boldsymbol{x}) \gamma(\boldsymbol{x}, \tau) n(\boldsymbol{x}, \tau, t) \tag{S5}$$

Let us denote

$$\mathbb{Q}_{\mathcal{X}} n(\boldsymbol{x}, \tau, t) = \sum_{\boldsymbol{x}' \in \mathcal{X}} q(\boldsymbol{x}, \boldsymbol{x}') n(\boldsymbol{x}', \tau, t) - q(\boldsymbol{x}', \boldsymbol{x}) n(\boldsymbol{x}, \tau, t). \tag{S6}$$

In addition, we keep track of the number of cells that exit the truncated state space $\bar{\mathcal{X}}$ via the following evolution equation:

$$\partial_t m(\bar{\boldsymbol{x}}, \tau, t) = \sum_{\bar{\boldsymbol{x}} \in \bar{\mathcal{X}}} q(\bar{\boldsymbol{x}}, \boldsymbol{x}) n(\boldsymbol{x}, \tau, t). \tag{S7}$$

For brevity let us denote $\sum_{\bar{\boldsymbol{x}} \in \bar{\mathcal{X}}} q(\bar{\boldsymbol{x}}, \boldsymbol{x}) = \bar{q}(\boldsymbol{x})$. Note that the sum above is taken over a potentially infinite complement $\bar{\mathcal{X}}$. However, in practice when constructing the models based on a defined stochastic reaction network we can often easily find the total rate $q(\boldsymbol{x})$ corresponding to reactions leaving the state $\boldsymbol{x} \in \mathcal{X}$. Further, we can also compute the total rate $\sum_{\boldsymbol{x}' \in \mathcal{X}} q(\boldsymbol{x}', \boldsymbol{x})$ of transitioning from $\boldsymbol{x}$ to another state within the truncation $\mathcal{X}$. We then use that $q(\boldsymbol{x}) = \sum_{\boldsymbol{x}' \in \mathcal{X}} q(\boldsymbol{x}', \boldsymbol{x}) + \bar{q}(\boldsymbol{x})$ to evaluate the $\bar{q}(\boldsymbol{x})$ without having to sum over the infinite complement $\bar{\mathcal{X}}$.

To make analytical progress we consider the asymptotic behaviour of the defined system in the regime where the population grows exponentially with doubling rate λ. In particular, $n(\boldsymbol{x},\tau,t) \sim e^{\lambda t}\Pi(\boldsymbol{x},\tau)$ and $m(\bar{\boldsymbol{x}},\tau,t) \sim e^{\lambda t}\pi(\boldsymbol{x},\tau)$ where Π and π are the snapshot densities of cells within the truncated state space and outside of it respectively. In the exponential growth regime the number of cells crossing the truncation boundary can then be given by

$$\lambda\pi(\boldsymbol{x},\tau) = \bar{q}(\boldsymbol{x})\Pi(\boldsymbol{x},\tau). \tag{S8}$$

The additional source of error that needs to be considered is the finite time interval for integrals involving cell age. Let us fix a finite time interval $[0,\tau_{\max}]$. The proposed method then reinitialised both the cells that leave the truncation $\mathcal{X}$ and cells that do not divide in the finite time interval $[0,\tau_{\max}]$ according to the division kernel as newborn cells. Thus, we get the following system

$$(\lambda + \partial_\tau + \gamma(\boldsymbol{x},\tau))\Pi(\boldsymbol{x},\tau) = \mathbb{Q}_{\mathcal{X}}\Pi(\boldsymbol{x},\tau) \tag{S9}$$

$$\Pi(\boldsymbol{x},0) = m\int_0^{\tau_{\max}} d\tau \sum_{\boldsymbol{x}'\in\mathcal{X}} K(\boldsymbol{x}|\boldsymbol{x}')\left[\gamma(\boldsymbol{x}',\tau) + \frac{1}{m}\bar{q}(\boldsymbol{x}')\right]\Pi(\boldsymbol{x}',\tau) + \sum_{\boldsymbol{x}'\in\mathcal{X}} K(\boldsymbol{x}|\boldsymbol{x}')\Pi(\boldsymbol{x}',\tau_{\max}). \tag{S10}$$

We then consider the conditional distribution $\Pi(\boldsymbol{x}|\tau) = \frac{\Pi(\boldsymbol{x},\tau)}{\Pi(\tau)}$. Substituting this into the joint evolution (Equation S9) and noting that the age-dependent marginal evolution is given by

$$(\partial_\tau + \lambda + \gamma(\tau))\Pi(\tau) = 0 \tag{S11}$$

gives us

$$(\partial_\tau + \gamma(\boldsymbol{x},\tau) - \gamma(\tau))\Pi(\boldsymbol{x}|\tau) = \mathbb{Q}_{\mathcal{X}}\Pi(\boldsymbol{x}|\tau) \tag{S12}$$

where $\gamma(\tau)$ is the marginal division rate $\mathbb{E}_{\Pi(\boldsymbol{x}|\tau)}[\gamma(\boldsymbol{x},\tau)]$. We note that

$$(\partial_\tau + \gamma(\boldsymbol{x},\tau))\Pi'(\boldsymbol{x}|\tau) = \mathbb{Q}_{\mathcal{X}}\Pi'(\boldsymbol{x}|\tau) \tag{S13}$$

then describes the density of cells that have not divided yet leading to the first passage time distribution for a cell to divide from trait $\boldsymbol{x}$ at time τ, division distribution for brevity, given by

$$\nu(\boldsymbol{x},\tau) = me^{-\lambda\tau}\gamma(\boldsymbol{x},\tau)\Pi'(\boldsymbol{x}|\tau). \tag{S14}$$

Again by the definition of conditional distribution we can then derive the boundary condition for the conditional evolution as

$$\Pi(\boldsymbol{x}|0) = \sum_{\boldsymbol{x}'\in\mathcal{X}} K(\boldsymbol{x}|\boldsymbol{x}')\left[\int_0^{\tau_{\max}} d\tau\left[\nu(\boldsymbol{x}',\tau) + e^{-\lambda\tau}\bar{q}(\boldsymbol{x}')\Pi'(\boldsymbol{x}'|\tau)\right] + e^{-\lambda\tau_{\max}}\Pi'(\boldsymbol{x}'|\tau_{\max})\right]. \tag{S15}$$

The exit probability

$$\varepsilon(\boldsymbol{x}',\lambda) = \int_0^{\tau_{\max}} d\tau e^{-\lambda\tau}\bar{q}(\boldsymbol{x}')\Pi'(\boldsymbol{x}'|\tau) + e^{-\lambda\tau_{\max}}\Pi'(\boldsymbol{x}'|\tau_{\max}) \tag{S16}$$

corresponds to the cells leaving the truncation from state $\boldsymbol{x}'$ and dividing within the finite time horizon $[0,\tau_{\max}]$. Note that summing over $\boldsymbol{x}' \in \mathcal{X}$ corresponds to the total exit probability ε for a cell to leave the state space

$$\varepsilon(\lambda) = \int_0^{\tau_{\max}} d\tau e^{-\lambda\tau}\sum_{\boldsymbol{x}\in\mathcal{X}} \bar{q}(\boldsymbol{x})\Pi'(\boldsymbol{x}|\tau) + e^{-\lambda\tau_{\max}}\sum_{\boldsymbol{x}\in\mathcal{X}}\Pi'(\boldsymbol{x}|\tau_{\max}). \tag{S17}$$

This takes into account truncation as well as the finite time-horizon used to compute the transient evolution of $\Pi'(\boldsymbol{x}|\tau)$. Summing the boundary condition over $\boldsymbol{x}$ then gives

$$1 = m\int_0^{\tau_{\max}} d\tau e^{-\lambda\tau}\nu(\tau) + \varepsilon(\lambda) \tag{S18}$$

In the solution algorithm, presented in the Methods section of the main text, the equations (S15) and (S18) are computed at every iteration step.

Note that if $\varepsilon(\boldsymbol{x},\lambda) = 0$ for all $\boldsymbol{x} \in \mathcal{X}$ then the boundary condition for the population lineage trees described in the main text by Equations (1) is recovered. Moreover

$$1 = m\int_0^{\infty} d\tau e^{-\lambda\tau}\nu(\tau) \tag{S19}$$

would correspond to the Euler-Lotka equation for the population lineage trees in the case of the untruncated state space and the time horizon $[0,\infty]$.

S3. TELEGRAPH MODEL

In this section we provide the complete specification of the agent-based telegraph model used in the main manuscript. The intracellular dynamics are given by the following stochastic reaction network

$$
\begin{aligned}
&G_{off} \xrightarrow{k_{on}} G_{on} \\
&G_{on} \xrightarrow{k_{off}} G_{off} \\
&G_{on} \xrightarrow{k_{prod}} G_{on} + m \times x \\
&x \xrightarrow{k_{deg}} \emptyset
\end{aligned}
$$

where $m \sim Geometric(b)$ is a geometrically distributed random variable parametrised by the mean b. In practice, to simplify the implementation with Julia Catalyst package [SI3] the bursty reaction was truncated and split into multiple reactions

$$
\begin{aligned}
&G_{on} \xrightarrow{p(1)k_{prod}} G_{on} + 1 \times x \\
&\dots \\
&G_{on} \xrightarrow{p(N)k_{prod}} G_{on} + N \times x
\end{aligned}
$$

where the rate of each reaction is weighed by the probability density p of the burst size. Note that the truncation of the bursty reaction is not necessary for the computations of $\bar{q}$ in Section S2. The total rate out of the each state with gene on and protein count x is the sum of k_{off}, k_{deg} and k_{prod}. Thus all we need to find the rate corresponding to cells leaving the truncation is to consider the cumulative probability of bursts that do not leave the truncation.

In the case of neutral condition with no selection the division rate is given by $\gamma(\boldsymbol{x}, \tau) = g(\tau)$ where $g(\tau)$ is the hazard of the Gamma distribution parametrised by mean its m and squared coefficient of variation cv^2. In general, if f and F are the probability density and cumulative distribution functions of a distribution respectively, then the hazard of the distribution is defined by

$$
g(\tau) = \frac{f(\tau)}{1 - F(\tau)}. \tag{S20}
$$

In the selection case the division rate is given by $\gamma(\boldsymbol{x}, \tau) = s(\boldsymbol{x})g(\tau)$ where $s(x)$ is a Hill function

$$
s(\boldsymbol{x}) = \frac{x^n}{K^n + x^n}. \tag{S21}
$$

The chosen parameters are given in the table below.

k_{on}	k_{off}	k_{prod}	mean burst size b	k_{deg}	$Gamma(m, cv^2)$	Hill exponent n	Hill coefficient K
0.7	0.2	20.0	1.2	0.1	$(0.8595, 0.6)$	2	20

S4. FEEDBACK MODELS

A. Transcriptional feedback model

Agent-based model. The intracellular dynamics of the agent-based model are given by the following stochastic reaction network

$$
\emptyset \xrightarrow{\Omega\alpha + \Omega k(x^2/(K\Omega^2 + x^2))} x
$$

where the protein x promotes its own production. The division rate function is given as the hazard of the Gamma distribution parametrised by its mean m and the squared coefficient of variation cv^2. Let f and F denote the probability density and cumulative distribution functions of the Gamma distribution respectively. The division rate $\gamma(x, \tau)$ is then given by

$$
\gamma(x, \tau) = g(\tau) = \frac{f(\tau)}{1 - F(\tau)}. \tag{S22}
$$

The partitioning of mother cell molecule numbers at division follows symmetric binomial partitioning.

Effective dilution model In the effective dilution model we add a linear dilution term to the stochastic reaction network

$$\emptyset \xrightarrow{\Omega\alpha+\Omega k(x^2/(K\Omega^2+x^2))} x$$
$$x \xrightarrow{\lambda} \emptyset.$$

The degradation parameter λ models the loss of protein due to cell divisions in a population growing exponentially with doubling time λ. The parametrisation of the gamma distribution is chosen to result in this doubling rate. The stationary solutions for the birth-death processes arising from the effective dilution models were computed using standard steady state methods [SI1].

Parametrisation The chosen parameters are given in the table below.

α	k	Hill coefficient K	Ω	λ	$Gamma(m, cv^2)$
$\{0.0, 0.5, \cdots, 0.7\}$	6.0	10.0	10.0	1.0	$(0.7177, 0.1)$

B. Positive growth feedback model

Agent-based model. We provide the complete specifications of the growth feedback models used in the main manuscript. The intracellular dynamics of the agent-based model are given by the following stochastic reaction network

$$\emptyset \xrightarrow{\Omega\alpha} x$$
$$x \xrightarrow{\lambda} \emptyset.$$

The division rate function is given by a Hill function dependent on the protein counts

$$\gamma(x, \tau) = s(x) = kx(K\Omega^2/(K\Omega^2 + x^3)).$$

The partitioning of mother cell molecule numbers at division follows symmetric binomial partitioning.

Effective dilution model. In the effective dilution model we add a dilution term corresponding to the division rate to the stochastic reaction network

$$\emptyset \xrightarrow{\Omega\alpha} x$$
$$x \xrightarrow{\lambda+k(K\Omega^2/(K\Omega^2+x^3))} \emptyset.$$

Parametrisation. The chosen parameters are given in the table below.

α	k	Hill coefficient K	Ω	λ
$\{1.5, 2.0, \cdots, 6.0\}$	20.0	1.0	10.0	1.0

C. Combined feedback model

Agent-based model. The feedback model in this section combines the transcriptional feedback model (Section S4 A) and growth feedback (Section S4 B). Thus, the intracellular dynamics of the agent-based model are given by the following stochastic reaction network

$$\emptyset \xrightarrow{2\Omega\alpha+\Omega k_1(x^2/(K_1\Omega^2+x^2))} x$$
$$x \xrightarrow{\lambda} \emptyset.$$

The division rate function is similar to growth feedback model (with higher Hill exponent) and is given by a Hill function dependent on the protein counts

$$\gamma(x, \tau) = s(x) = k_2 x(K_2\Omega^2)/(K_2\Omega^2 + x^4).$$

The partitioning of mother cell molecule numbers at division follows symmetric binomial partitioning.

Effective dilution model. In the effective dilution model we add a corresponding dilution term to the stochastic reaction network

$$\emptyset \xrightarrow{2\Omega\alpha+\Omega k_1(x^2/(K_1\Omega^2+x^2))} x$$
$$x \xrightarrow{\lambda} \emptyset$$
$$x \xrightarrow{k_2(K_2\Omega^2/(K_2\Omega^2+x^4))} \emptyset.$$

Parametrisation. The chosen parameters are given in the table below.

α	k_1	Hill coefficient K_1	k_2	Hill coefficient K_2	Ω	λ
$\{4.2, 4.3, \cdots, 4.8\}$	80.0	4.0	40.0	15.0	70.0	25.0

S5. PARAMETER AND DIVISION RATE INFERENCE

A. Conversion factor

The *Escherichia coli* datasets [SI2, SI4] analysed in the main text report fluorescence intensity of the reporter protein. In order to fit the agent-based model to data we convert the intensity to copy numbers of the protein by analysing the variability in the mother and daughter cell fluorescences at division as done, for example, in [SI5]. To that end we find a linear relationship $f = \alpha x$ between the copy numbers of fluorescent molecules x and fluorescence intensity f. This conversion is done under the assumption that partitioning of the fluorescent molecules between the two daughter cells at division is binomial with probability $p = \frac{1}{2}$. Variance of the daughter cell fluorescence f_d is then given by

$$Var(f_d) = Var(\alpha x_d) = \alpha^2 p(1-p)x_m = \frac{\alpha}{4} f_m$$

where x_m and f_m are the molecule count and fluorescence of the mother cell respectively. From the data we then fit the slope a of $Var(f_d) = a f_m$ and equate it with $\frac{\alpha}{4}$ to estimate the conversion factor α.

B. DNA damage response model

The intracellular dynamics of the agent-based model are given by the following stochastic reaction network

$$\emptyset \xrightarrow{k} m \times x$$

where $m \sim Geometric(b)$ is a geometrically distributed random variable parametrised by the mean b (see Section S3 for implementation details). In the wild type case the division rate is given by $\gamma(x, \tau) = g(\tau)$ where $g(\tau)$ is the hazard of the kernel density estimate of the interdivision times in the data. If f and F denote the probability density and cumulative distribution functions of the kernel density estimate

$$g(\tau) = \frac{f(\tau)}{1 - F(\tau)}. \tag{S23}$$

In the induced DNA damage case the division rate is given by $\gamma(x, \tau) = s(x)g(\tau)$ where $s(x)$ is a Hill function

$$\frac{L(1-\delta)x^m}{(K^m + x^m) + \delta)}. \tag{S24}$$

The partitioning of mother cell molecule numbers at division follows symmetric binomial partitioning. The parameters fitted via Bayesian Optimisation are given in the table below.

	k	b	L	K	δ	m
Wild type	0.2070	1.4643	N/A	N/A	N/A	N/A
DNA damage	0.2070	1.4643	1.0469	44.68	0.0	11

C. Antibiotic resistance model

The intracellular dynamics of the agent-based model are given by the following stochastic reaction network

$$\emptyset \xrightarrow{k} m \times x$$

where k is the burst frequency and $m \sim \mathit{Geometric}(b)$ is a geometrically distributed random variable parametrised by the mean burst size b (see Section S3 for implementation details). In the *no treatment* case the division rate is given by $\gamma(x, \tau) = g(\tau)$ where $g(\tau)$ is the hazard of the kernel density estimate of the interdivision times in the data. If f and F denote the probability density and cumulative distribution functions of the kernel density estimate

$$g(\tau) = \frac{f(\tau)}{1 - F(\tau)}. \tag{S25}$$

In the *treatment* case the division rate is given by $\gamma(x, \tau) = s(x)g(\tau)$ where $s(x)$ is a Hill function

$$s(x) = \frac{L(1-\delta)x^m}{(K^m + x^m) + \delta)}. \tag{S26}$$

The partitioning of mother cell molecule numbers at division follows symmetric binomial partitioning. The parameters fitted via Bayesian Optimisation are given in the table below.

	k	b	L	K	δ	m
No treatment	0.5684	1.4087	N/A	N/A	N/A	N/A
Treatment (selection)	0.5684	1.4087	1.2336	70.4	0.0	20
Treatment (selection + adaptation)	0.3378	2.0725	1.4643	92.8	0.0	4

[SI1] C. Gardiner. *Stochastic Methods: A Handbook for the Natural and Social Sciences*. Springer Series in Synergetics. Springer Berlin Heidelberg, 2009. ISBN 978-3-540-86684-8.

[SI2] Sebastián Jaramillo-Riveri, James Broughton, Alexander McVey, Teuta Pilizota, Matthew Scott, and Meriem El Karoui. Growth-dependent heterogeneity in the dna damage response in escherichia coli. *Molecular Systems Biology*, 18(5):e10441, 2022. doi:10.15252/msb.202110441.

[SI3] T. Loman, Y. Ma, V. Ilin, S. Gowda, N. Korsbo, N. Yewale, C. V. Rackauckas, and S. A. Isaacson. Catalyst: Fast biochemical modeling with julia. *bioRxiv*, 2022. doi:10.1101/2022.07.30.502135.

[SI4] Takashi Nozoe, Edo Kussell, and Yuichi Wakamoto. Inferring fitness landscapes and selection on phenotypic states from single-cell genealogical data. *PLOS Genetics*, 13(3):1–25, March 2017. doi:10.1371/journal.pgen.1006653. Publisher: Public Library of Science.

[SI5] Nitzan Rosenfeld, Jonathan W. Young, Uri Alon, Peter S. Swain, and Michael B. Elowitz. Gene Regulation at the Single-Cell Level. *Science*, 307(5717):1962–1965, March 2005. doi:10.1126/science.1106914. Publisher: American Association for the Advancement of Science.

[SI6] Philipp Thomas. Making sense of snapshot data: ergodic principle for clonal cell populations. *Journal of The Royal Society Interface*, 14(136):20170467, 2017. doi:10.1098/rsif.2017.0467.

[SI7] Philipp Thomas. Intrinsic and extrinsic noise of gene expression in lineage trees. *Scientific Reports*, 9(1):474, January 2019. ISSN 2045-2322. doi:10.1038/s41598-018-35927-x.

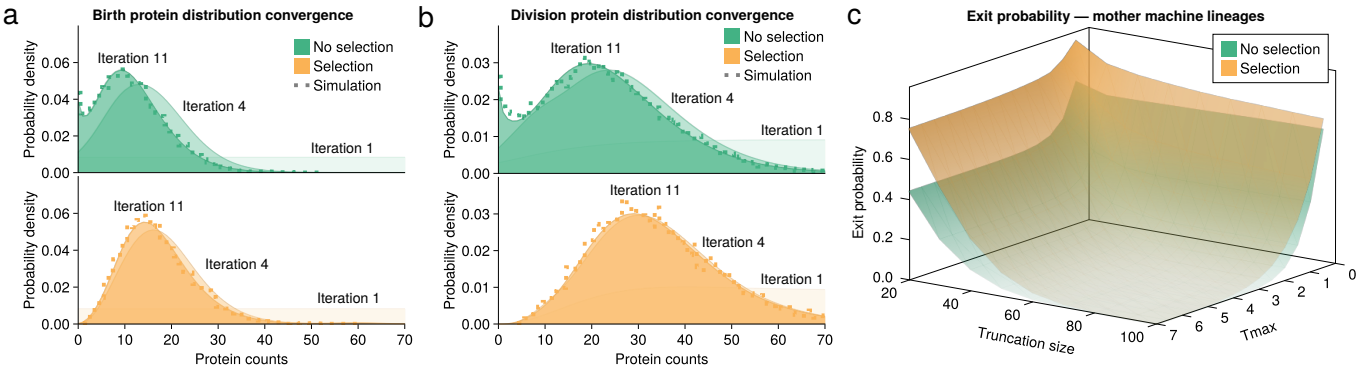

FIG. S1. Convergence of the mother machine lineage statistics of the telegraph model. **(a-b)** Birth (panel **a**) and division (panel **b**) distributions of the mother machine lineage model with fixed a truncation size and $\tau_{\max}$ converges in a couple of iterations and agrees with the agent-based simulation. **(c)** The exit probability due to the FSP truncation decreases with the truncation size and time horizon $\tau_{\max}$.

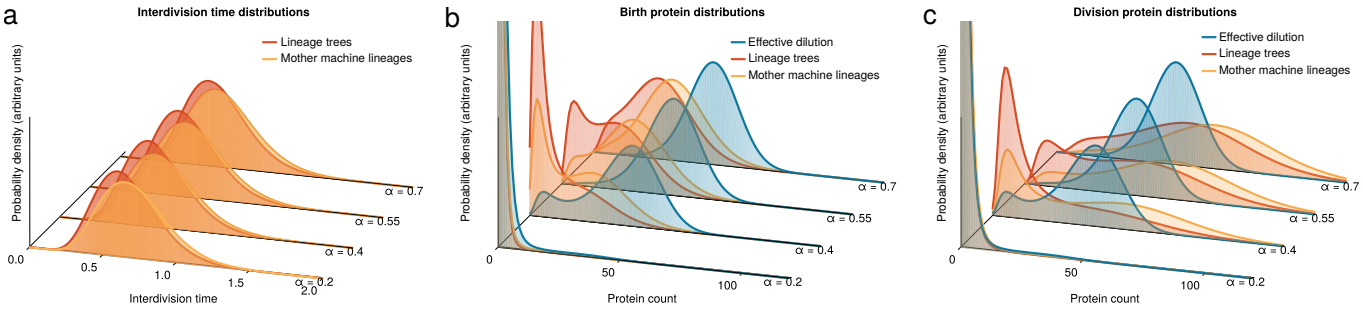

FIG. S2. Summary distributions of the transcriptional feedback model. **(a)** The interdivision time distribution shows slow dividing cells being over-represented in mother machine lineages (yellow) compared to population lineage trees (red). **(b-c)** Protein distributions predicted by the agent-based models at birth (panel **b**) and division (panel **c**) are compared with the stationary distribution of the effective dilution model.

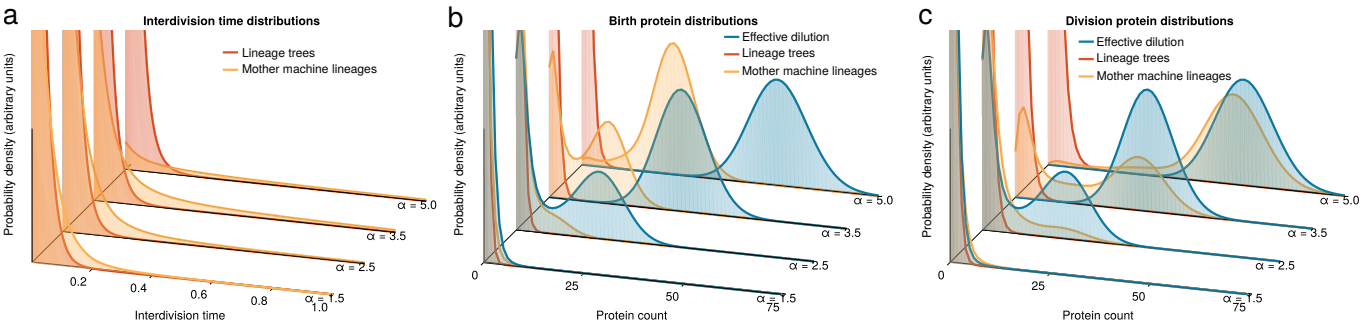

FIG. S3. Summary distributions of the growth feedback model. **(a)** The interdivision time distribution shows slow dividing cells are over-represented in mother machine lineages (yellow) compared to the population lineage trees (red). The right tail of the unimodal interdivision time distribution corresponding to the mother machine lineages becomes longer as the protein production rate α increases. The corresponding slow dividing cells are repressed in the lineage tree statistics. **(b-c)** Protein distributions predicted by the agent-based models at birth (panel **b**) and division (panel **c**) are compared with the stationary distribution of the effective dilution model.

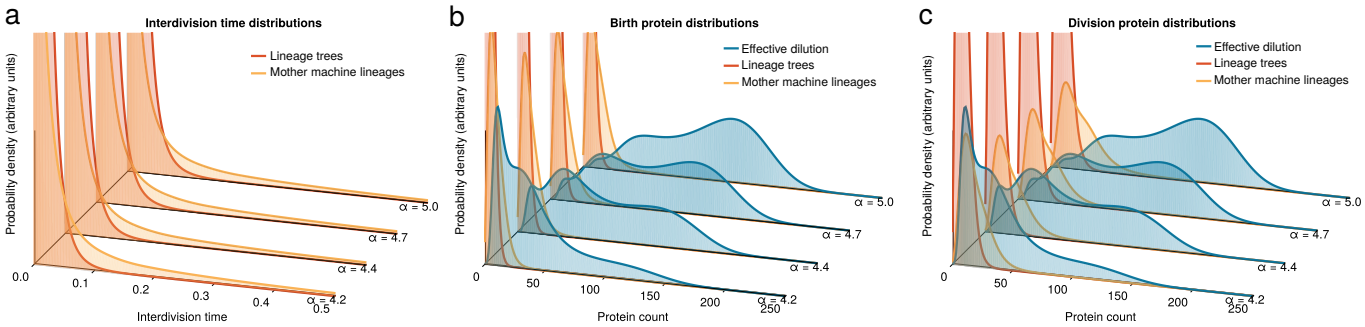

FIG. S4. Summary distributions of the model combining transcriptional and growth feedback mechanism. **(a)** The interdivision time distributions display the behaviour observed for the growth feedback model (Figure S3a) with the right tail of the unimodal interdivision time distribution becoming longer as the synthesis rate α increases. As before the corresponding slow dividing cells are repressed in the lineage tree statistics. **(b-c)** Protein distributions predicted by the agent-based models at birth (panel **b**) and division (panel **c**) are compared with the stationary distribution of the effective dilution model.

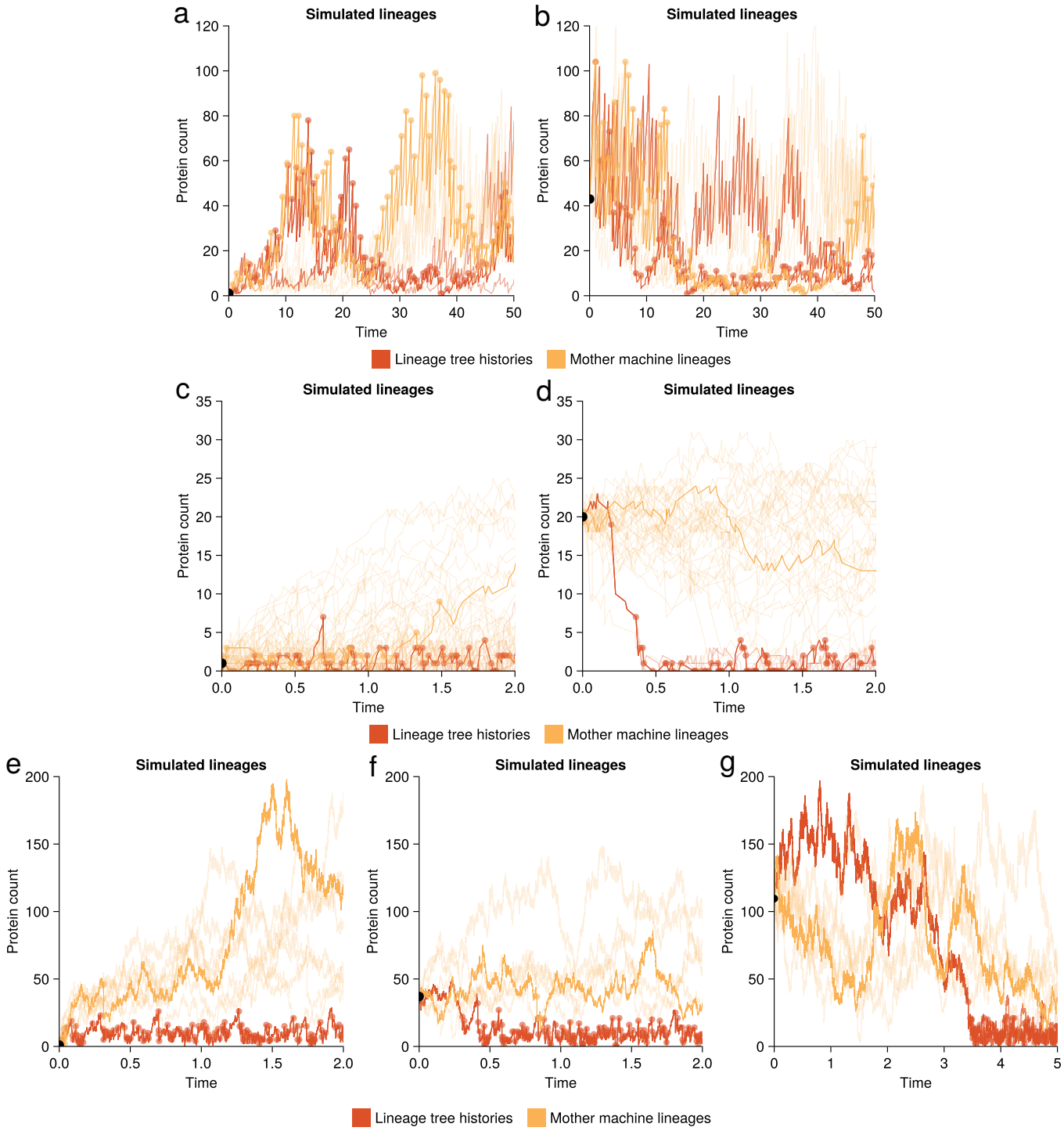

FIG. S5. Agent-based stochastic simulations of lineage tree histories (red) and mother cell lineages (yellow). **(a-b)** Simulations of transcriptional feedback model (model details in SI Section S4 A) for $\alpha = 4.0$. Agent-based simulations with cells initialised in a low expression level state (1 molecule, panel **a**) and a high expression level state (20 molecule, panel **b**). Lineage tree histories and mother machine lineages explore both the high expression and low expression states under both initialisations. **(c-d)** Simulations of the growth feedback model (model details in SI Section S4 B) for $\alpha = 2.0$. **c** Agent-based simulations initialised with cells in a low expression level fast dividing state (1 molecule). The lineage tree histories remain in their initial fast dividing state while mother machine lineages eventually visit the slow dividing state. **d** Agent-based simulations initialised with cells in a high expression level state (20 molecules). Lineage tree histories show strong selection for the fast dividing cell lineages in a population with histories coming down to the low expression fast dividing state in a couple of divisions. The histories resulting from cells that quickly make the transition to fast dividing regime are going to be highly represented in lineage tree histories. **(e-g)** Simulations of the combined feedback model (model details in SI Section S4 C) for $\alpha = 4.4$. Agent-based simulations with cells initialised in a low expression level state (1 molecule, panel **e**) and two high expression level states (37 molecules in panel **f**, 111 molecules in panel **g**). On short time scales the mother machine lineages and lineage tree histories agree with the qualitative dynamics of each other. However, over time the lineage tree histories settle in the fast dividing cell state.

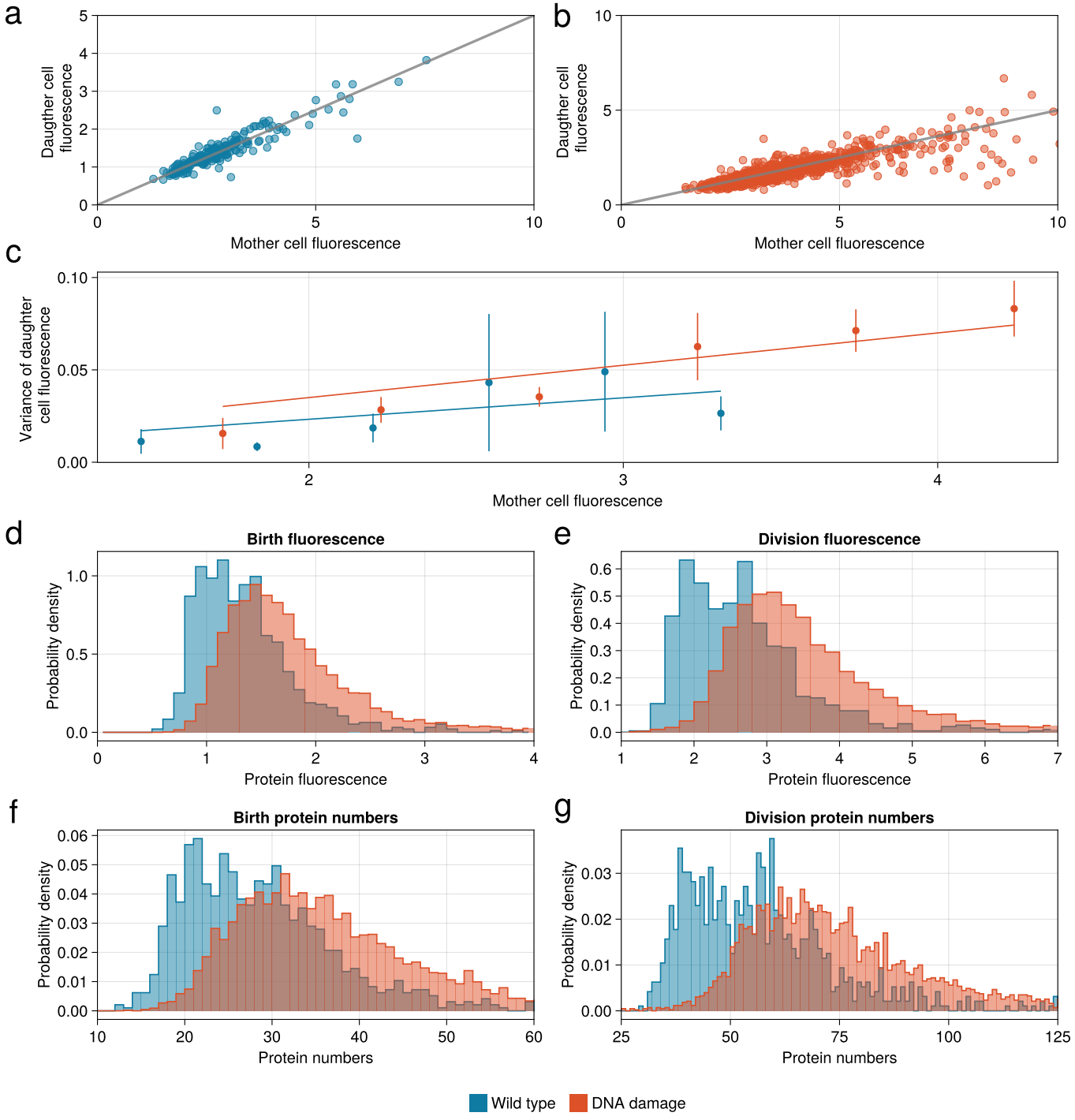

FIG. S6. Conversion factor estimation for the DNA damage response dataset. **(a-b)** The partitioning of fluorescence between the mother and daughter cells compared against symmetric partitioning (gray line with slope 0.5). **(c)** Linear regression lines for the binned mother cell fluorescence values against the variance of the daughter cell fluorescence within the bin. Scatter points represent the midpoints of the bins. The slope of the wild type case is chosen as the conversion factor. **(d-e)** Histograms displaying the birth (panel **d**) and division (panel **e**) fluorescence distributions of the wild type (blue) and the induced DNA damage strain (red) from the data. **(f-g)** Histograms showing the birth (panel **f**) and division (panel **g**) protein distribution resulting from the estimated conversion factor.

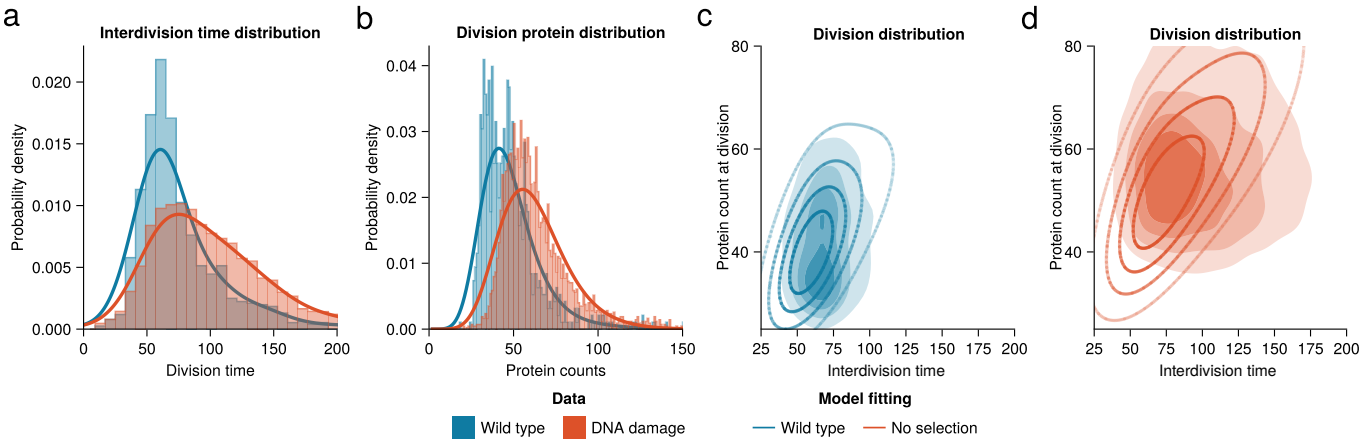

FIG. S7. Changes in the division rate without selection effects do not capture the SOS response dynamics observed in the data. **(a)** Interdivision time distributions for the two conditions are fitted by a separate kernel density estimate. **(b)** With the gene expression dynamics kept constant between the conditions the division protein distribution is well captured by the model. **(c-d)** Comparison of the division distributions of the wild type (panel **c**) and damage-induced (panel **d**) cells from the data with the mother machine lineage division distribution. The model overestimates the correlation between the protein count and interdivision time for the damage-induced cells.

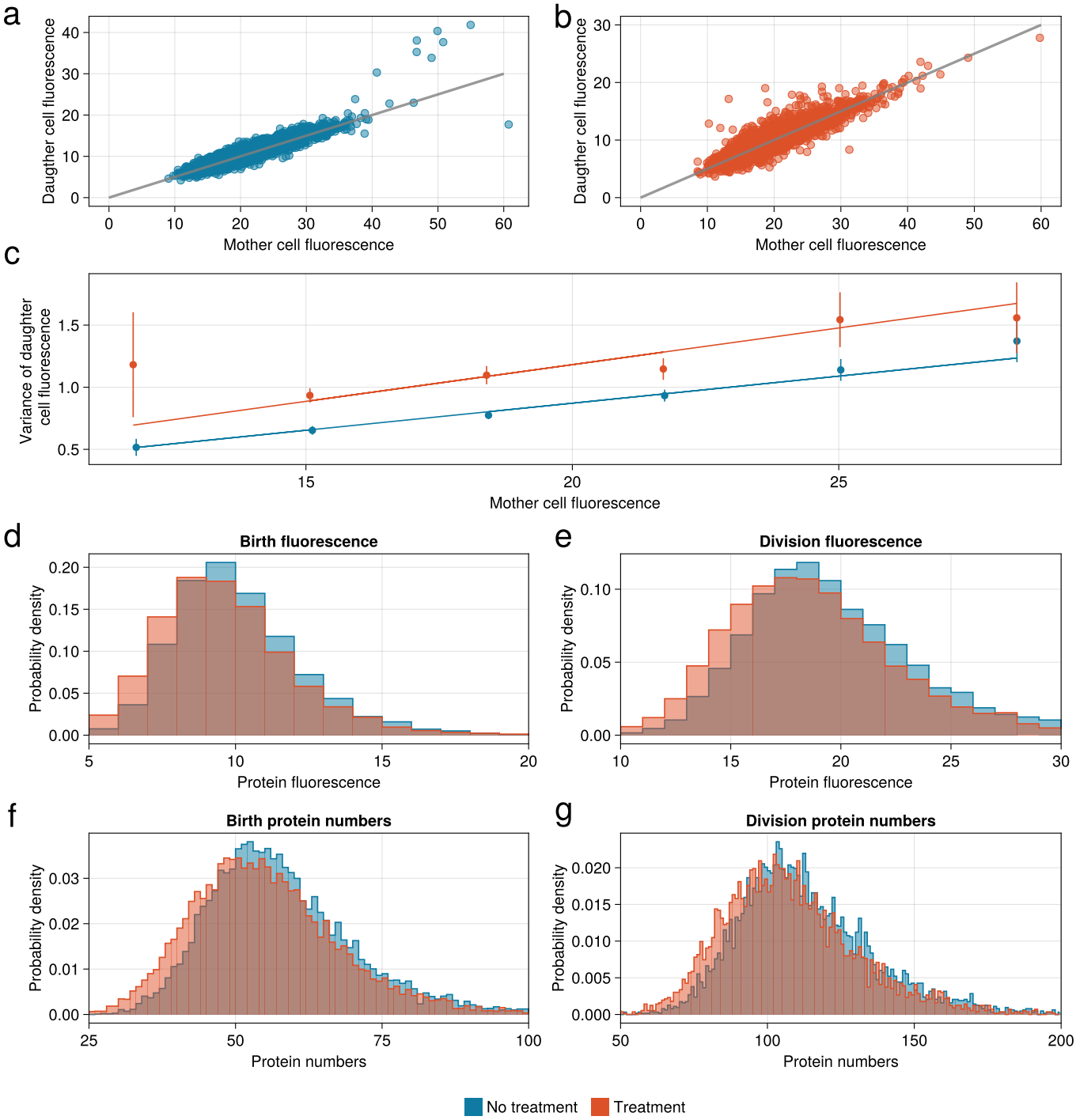

FIG. S8. Conversion factor estimation for the DNA damage response dataset. **(a-b)** The partitioning of fluorescence between the mother and daughter cells compared against symmetric partitioning (gray line with slope 0.5). **(c)** Linear regression lines for the binned mother cell fluorescence values against the variance of the daughter cell fluorescence within the bin. Scatter points represent the midpoints of the bins. The slope of the no treatment case is chosen as the conversion factor. **(d-e)** Histograms displaying the birth (panel **d**) and division (panel **e**) fluorescence distributions of the untreated (blue) and with antibiotic-treated (red) cells from the data. **(f-g)** Histograms showing the birth (panel **f**) and division (panel **g**) protein distribution resulting from the estimated conversion factor.

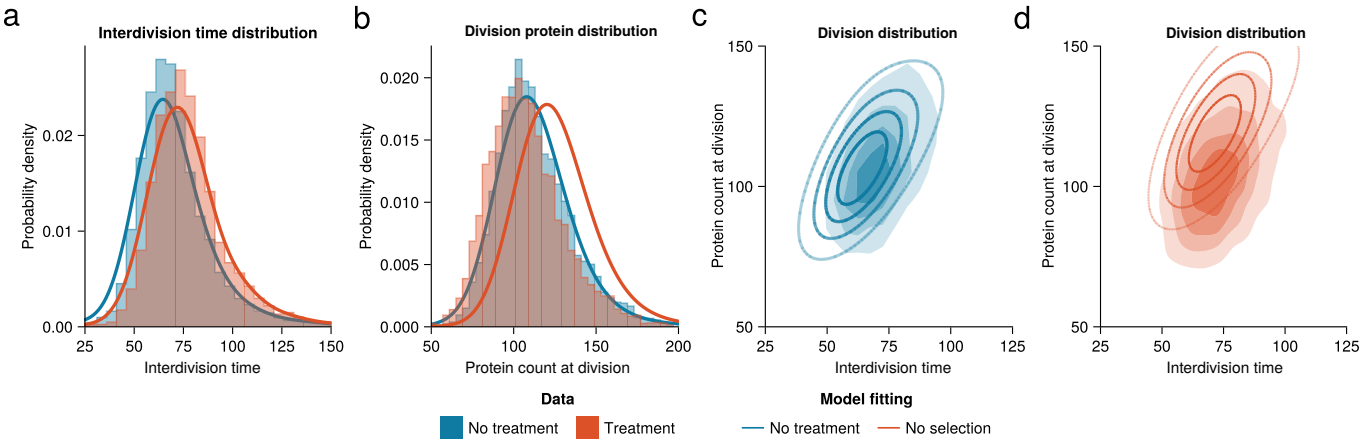

FIG. S9. Changes in the division rate alone are not sufficient to capture the antibiotic treatment response of *Escherichia coli* cells. **(a)** Interdivision time distributions of for conditions are fitted by a separate kernel density estimate. **(b)** With the gene expression dynamics kept constant between the conditions the model predicts significantly higher division protein counts than observed in the antibiotic-treated data. **(c-d)** Comparison of the division distributions of untreated (panel **c**) and antibiotic-treated (panel **d**) cells from the data with the corresponding agent-based lineage tree division distributions.